

Anisotropic flow and the valence quark skeleton of hadrons

Meijian Li,^{1,*} Wenyang Qian,^{1,†} Bin Wu,^{1,‡} and Hong Zhang^{2,§}

¹*Instituto Galego de Física de Altas Enerxías IGFAE,*

Universidade de Santiago de Compostela, E-15782 Galicia-Spain

²*Institute of Frontier and Interdisciplinary Science,*

Key Laboratory of Particle Physics and Particle Irradiation (MOE),

Shandong University, Qingdao, Shandong 266237, China

We study transverse momentum anisotropies, in particular, the elliptic flow v_2 due to the interference effect sourced by valence quarks in high-energy hadron-hadron collisions. Our main formula is derived as the high-energy (eikonal) limit of the impact-parameter dependent cross section in quantum field theory, which agrees with that in terms of the impact parameter in the classical picture. As a quantitative assessment of the interference effect, we calculate v_2 in the azimuthal distribution of gluons at a comprehensive coverage of the impact parameter and the transverse momentum in high-energy pion-pion collisions. In a broad range of the impact parameter, a sizable amount of v_2 , comparable with that produced due to saturated dense gluons or final-state interactions, is found to develop. In our calculations, the valence sector of the pion wave function is obtained numerically from the Basis Light-Front Quantization, a non-perturbative light-front Hamiltonian approach. And our formalism is generic and can be applied to other small collision systems like proton-proton collisions.

* meijian.li@usc.es

† qian.wenyang@usc.es

‡ b.wu@cern.ch

§ hong.zhang@sdu.edu.cn

I. INTRODUCTION

In heavy-ion collisions, azimuthal anisotropies have long been viewed as one of the major signatures for the formation of strongly-coupled quark-gluon plasma (QGP) fluid droplets [1]. The unexpected observations of collectivity in proton-proton (pp) and proton-nucleus (pA) collisions [2–23] have, however, put such a QGP signature under intense scrutiny and inspired extensive exploration of other potential sources for collectivity in the past decade (see refs. [24, 25] for recent reviews). Pinning down the true origin of collectivity in small collision systems is one of the major goals to be pursued by the heavy-ion community in the decades to come [26].

Extending the hydrodynamic paradigm in heavy-ion collisions to small collision systems has yielded some phenomenological success in explaining experimental data as pioneered in refs. [27–29]. Its applicability has thus far been justified to some extent by studies in microscopic models which concluded the dominance of hydrodynamic modes in systems comparable to, or even considerably smaller than, the proton size as summarized in [30]. On the other hand, it is yet to be understood how hydrodynamization could be established in such small systems from QCD first principles. Moreover, sizable momentum anisotropies can already be produced via one final-state interaction as shown in kinetic theory [31–35] or via color reconnection in PYTHIA [36], which all indicates that hydrodynamics, if present, may not be solely responsible for collectivity in small collision systems [37–41].

Without considering any final-state interactions, transverse momentum anisotropies could also be produced in pp and pA collisions. Various initial-state correlations responsible for such momentum anisotropies have been intensively investigated in parton saturation physics, i.e., the Color-Glass Condensate (CGC) [42–69]. Many of these studies (see, e.g., [56–69]) were focused on the dilute-dense limit in which only one of the two colliding particles is modelled as a saturated dense gluon state while the other (the proton) is treated as dilute. As an alternative mechanism without explicitly resorting to high initial parton saturation, interference between gluon waves emitted by various classical sources in hadrons has been shown to be capable of generating significant azimuthal asymmetries (in higher-order cumulants) as well [70, 71]¹.

Most of the above studies suffer from uncertainties due to some ad hoc modeling of color

¹ The approach to the interference effect in these works, otherwise, shares some commonalities with the glasma graph approach in CGC [53].

sources (large- x partons)². We note that the needed information on color sources or multiparton distributions could also be acquired from hadron wave functions evaluated in the following approaches: The light-front Hamiltonian formalism describes the hadron internal structure and dynamics through the light-front wavefunctions (LFWFs), which are fully relativistic and nonperturbative [73]. The basis light-front quantization (BLFQ) approach emerges as a computational framework to solve bound-state problems by employing basis representations [74]. The hadron LFWFs are obtained by diagonalizing the phenomenological effective Hamiltonian operator, which is based on light-front holography [75–77]. The application of BLFQ ranges from heavy mesons [78–81], heavy-light meson [82], light meson [83–87] and baryons [88–91]. The obtained LFWFs have provided us with opportunities to study various observables and physical processes.

In this paper we derive a formalism for studying high-energy hadron-hadron collisions from the impact-parameter dependent cross section in quantum field theory as defined in [92] and show that sizable transverse momentum anisotropies (mainly v_2) in soft gluon production can be produced due to the interference effect induced by the emitters of valence (anti)quarks in the dilute-dilute limit. Below, we explain the physical picture behind our calculations and summarize our main results.

The physical picture that motivates this work is as follows. Since we are mostly interested in low- p_T final-state hadrons which are not part of jets initiated by high- p_T partons, the relevant final-state partons (mostly gluons) typically have a transverse momentum $p_T \sim 1$ GeV and, equivalently, a de Broglie wavelength λ comparable with the transverse size of the colliding hadrons (~ 1 fm). Accordingly, their production is expected to be sensitive to the incoming color-singlet state of multipartons that are typically separated by a transverse distance $\sim \lambda$. In this case we expect that the most relevant multiparton state is given by the hadron valence quark skeleton as broadly assumed in parton saturation physics [93]. Motivated by the above expectation, we investigate below soft gluon production in the collisions of hadron valence quark skeletons as described by the LFWFs.

In sec. II, we present the main formula eq. (23) and the Feynman rules eq. (10) for calculating, order by order in perturbation theory, the gluon production in impact-parameter dependent hadron-hadron collisions. This formula is derived by taking the high collision energy (eikonal) limit of the impact-parameter dependent cross section defined in [92], as

² See ref. [72] and references therein for recent progress on this issue.

transcribed below in eq. (1). In this limit the dipole cross section for meson-meson collisions agrees with that broadly used in saturation/small- x physics [94–97]. This provides another verification of eq. (1) as a generic definition for the impact-parameter dependent cross section in quantum field theory, complementing to the hard (Drell-Yan) process studied in [92].

In sec. III we derive the meson-meson (mainly the dipole-dipole) cross section at leading order: first for inelastic forward scattering and then for one gluon production. With the latter result presented in eq. (35), we are able to study the momentum anisotropies of soft gluon production. In our gauge choice in which one meson does not radiate (to the midrapidity region), the cross section encodes the interference pattern of the two rays of gluon radiated respectively from the valence $q\bar{q}$ in the other meson. It is analogous to, though more sophisticated than, the classical double-slit experiment in optics, as discussed in detail in sec. IV. With such an analog in mind, this work shares some similarity with refs. [70, 71] as well as ref. [53], which dealt with a more intricate interference pattern among multiple gluons from multiple emitters.

Our main results of v_2 for pion-pion collisions follows in sec. V (see fig. 8). With the only two parameters in the meson LFWFs fixed by light meson masses as briefly reviewed in sec. VA, the results of v_2 at different impact parameters are shown and discussed in sec. VB. The main observations include: 1) Without any free parameters (except the impact parameter b) the magnitude of v_2 in the gluon production is typically comparable to that observed in pp collisions [10, 14, 15, 17, 18, 20, 22, 23] as well as theoretical results [25, 27, 28, 43, 47, 49, 51, 55, 57, 98–100]. 2) The interference pattern is found to manifest as a distinct, double-peak structure in v_2 for $b \gtrsim 0.1$ fm, which encodes the information on the hadron size.

II. THE IMPACT-PARAMETER DEPENDENT CROSS SECTION

Following refs. [45, 57], we investigate how transverse momentum anisotropies in the gluon production are correlated with the impact parameter of high-energy hadron-hadron collisions. We instead focus on the dilute-dilute limit, meaning both hadrons are taken as color-singlet multiparton states instead of saturated gluon states. In this section we derive the impact-parameter dependent cross section for producing partons of transverse momentum p_T in the limit $p_T \ll \sqrt{s}$, the center-of-mass (CM) energy of hadron-hadron

collisions.

A. The impact-parameter dependent cross section in the eikonal approximation

In quantum field theory the impact-parameter dependent cross section for the collision of two high-energy particles can be unambiguously defined as follows if the fuzziness in beam particles' transverse positions is much smaller than the impact parameter $b = |\mathbf{b}|$ [92]

$$\begin{aligned} \frac{d\sigma}{d^2\mathbf{b}dO} &= \int \prod_{i=A,B} \frac{d^2\mathbf{q}_i}{(2\pi)^2} e^{-i\mathbf{q}_i \cdot \mathbf{x}_i} \int \prod_f [d\Gamma_{p_f}] \delta(O - O(\{p_f\})) (2\pi)^2 \delta^{(2)}(\tilde{\mathbf{P}}_A + \tilde{\mathbf{P}}_B - \sum \mathbf{p}_f) \\ &\quad \times \frac{1}{2s} M(P_A, P_B \rightarrow \{p_f\}) M^*(\tilde{P}_A, \tilde{P}_B \rightarrow \{p_f\}) (2\pi)^4 \delta^{(4)}(P_A + P_B - \sum p_f), \end{aligned} \quad (1)$$

where $O(\{p_f\})$ defines an observable O as a function of the final-state momenta $\{p_f\}$, $M(P_A, P_B \rightarrow \{p_f\})$ is the amplitude for the process: $P_A, P_B \rightarrow \{p_f\}$, the phase-space measure for a particle of momentum p_f and mass m_f is defined as

$$\int d\Gamma_{p_f} \equiv \int \frac{d^4 p_f}{(2\pi)^4} (2\pi) \delta(p_f^2 - m_f^2) \theta(p_f^0), \quad (2)$$

in the CM frame the incoming momenta are given by

$$P_i^\mu = \frac{\sqrt{s}}{2} n_i^\mu + \frac{q_i^\mu}{2}, \quad \tilde{P}_i^\mu = \frac{\sqrt{s}}{2} n_i^\mu - \frac{q_i^\mu}{2} \quad (3)$$

with

$$n_A^\mu = (1, 0, 0, 1), \quad n_B^\mu = (1, 0, 0, -1), \quad q_i^\mu = (0, \mathbf{q}_i, 0) \quad (4)$$

and \mathbf{x}_i can be identified with the transverse location of hadron i in the classical picture with the impact parameter $\mathbf{b} \equiv \mathbf{x}_A - \mathbf{x}_B$. Here, all the terms of $O(q^2)$ or $O(m_i^2)$ with $i = A, B$ in the incoming momenta are neglected and two-dimensional transverse vectors are denoted by boldface letters.

For the production of high- p_T particles the underlying process is typically initiated by a binary collision of two partons respectively collinear to the two beam directions. In QCD this picture is manifest in the limit when the transverse coherent length of the collision $\sim 1/p_T$ is much shorter than the average separation between the partons in the hadrons $\sim 1/\Lambda_{QCD}$. In this case the cross section for the process takes a factorized form when expanded to the leading order in $1/p_T$, i.e., at leading twist. And the only information

of the hadron substructure encoded in such a hard process is, in general, the transverse phase-space distributions of single partons, referred to as thickness beam functions in [92].

Complementing to hard processes, we focus on the production of relatively low- p_T particles near midrapidity in the CM frame. At $p_T \sim 1$ GeV, the de Broglie wavelength of the produced particles $\lambda = 2\pi/p$ becomes comparable with the transverse size of the colliding hadrons. Accordingly, one may expect that the production of low- p_T particles is not sensitive to one but multipartons that are typically separated by a distance $\sim \lambda$ in the transverse plane inside the colliding hadrons. To substantiate such an expectation, below we make a detailed calculation of the azimuthal angle distribution of soft gluons produced in hadron-hadron collisions. In order to assess the sole importance of such an effect, we shall neglect other sources of azimuthal momentum anisotropies as recently reviewed in [24, 25].

We resort to the light-front wave functions (LFWFs) to decompose hadron states into color-singlet multiparton states [73] and focus on the valence sector of the hadron wave functions³. In this case our calculations boil down to the evaluation of the partonic cross section for soft gluon production in the collision of two color singlet states of valence (anti)quarks. Unlike the expansion of Feynman diagrams in p_T^{-1} for hard processes, we expand all the graphs in s^{-1} and keep only leading-order terms in s^{-1} . This corresponds to the so-called eikonal limit. The eikonal approximation has been broadly used in the Glauber model for heavy-ion collisions [101] and parton saturation physics [93]. Under this approximation we simplify the expression for the impact-parameter dependent cross section in eq. (1) and include below all ensuing Feynman rules for self-containment.

Our calculations are to be carried out in a mixed representation where longitudinal components of momenta and transverse coordinates are used to describe single particle states. Each valence (anti)quark carries a finite momentum fraction of its parent hadron and moves predominantly along the hadron's lightlike direction, denoted by n . In this case, the longitudinal components of their momentum p can be conveniently chosen to be $\bar{n} \cdot p$ and $n \cdot p$ with $\bar{n}^\mu \equiv (1, -\vec{n})$, which are respectively called the plus (“+”) and minus (“-”) components of p along n . That is, by definition a valence (anti)quark always carries a large plus momentum $\propto \sqrt{s}$ along n . By expanding in its plus momentum, Feynman rules associated

³ As broadly taken in parton saturation physics [93], this approximation is motivated by the observation that the valence quarks dominate at large x . The validity of such an approximation could be verified quantitatively by introducing one more collinear gluon in the Fock state (see, e.g., [87] for mesons and [72, 91] for the proton).

to the valence (anti)quark in the mixed representation reduce to

$$\begin{aligned}
\text{External quark lines:} \quad & \xrightarrow{p} \mathbf{x} = u_n^s e^{i\mathbf{p}\cdot\mathbf{x}} & \mathbf{x} \xrightarrow{p} & = \bar{u}_n^s e^{-i\mathbf{p}\cdot\mathbf{x}} \\
\text{External antiquark lines:} \quad & \xleftarrow{p} \mathbf{x} = \bar{v}_n^s e^{i\mathbf{p}\cdot\mathbf{x}} & \mathbf{x} \xleftarrow{p} & = v_n^s e^{-i\mathbf{p}\cdot\mathbf{x}} \\
\text{External gluon lines:} \quad & \xrightarrow{p} \mathbf{x} = \epsilon_\lambda(p) e^{i\mathbf{p}\cdot\mathbf{x}} & \mathbf{x} \xrightarrow{p} & = \epsilon_\lambda^*(p) e^{-i\mathbf{p}\cdot\mathbf{x}} \\
\text{Quark-gluon vertex:} \quad & \xrightarrow{\text{gluon}} \mathbf{x} = -igt^c \frac{\not{n}}{2} n^\mu \int d^2\mathbf{x} & & \\
\text{Gluon propagator:} \quad & \text{gluon} = \int \frac{d^2\mathbf{k}}{(2\pi)^2} \frac{-ig^{\mu\nu} e^{i\mathbf{k}\cdot(\mathbf{x}-\mathbf{y})}}{n\cdot p\bar{n}\cdot p - |\mathbf{k}|^2 + i\epsilon} & & \\
\text{Quark propagator:} \quad & \xrightarrow{p} \mathbf{x} = \frac{i\not{n}}{n\cdot p + i\bar{n}\cdot p \epsilon} & \xrightarrow{p} \mathbf{x} & = \frac{\not{n}}{2} (2\pi) \delta(n\cdot p) \delta^{(2)}(\mathbf{x}-\mathbf{y}).
\end{aligned} \tag{5}$$

In addition both the “+” and “-” momenta along n are conserved at each vertex. Since the momenta of valence (anti)quarks do not enter the observable O (near midrapidity), they are integrated out, giving rise to the delta function for the above cut fermion line. Here, the spinors with subscript n are defined for momentum $p^\mu = \frac{\bar{n}\cdot p}{2} n^\mu$.

Given a generic cut graph with the above Feynman rules, one can further make the following simplifications. Let us single out a cut fermion line corresponding to one valence (anti)quark:

$$S_q \equiv \text{diagram with a cut fermion line and gluon lines} \tag{6}$$

First, according to longitudinal momentum conservation and the Feynman rule for the cut fermion line, S_q contains the following delta functions:

$$2(2\pi) \delta(\bar{n}\cdot p - \bar{n}\cdot k - \bar{n}\cdot p') (2\pi) \delta^-\left(\sum_{i=1}^m n\cdot k_i\right) (2\pi) \delta^-\left(\sum_{i=1}^{m'} n\cdot k'_i\right), \tag{7}$$

where k is the total momentum of gluons in both the amplitude and the conjugate amplitude and the function δ^- is defined as

$$\delta^-\left(\sum_{i=1}^m n\cdot k_i\right) = \begin{cases} 1/(2\pi) & \text{for } m = 0 \\ \delta\left(\sum_{i=1}^m n\cdot k_i\right) & \text{for } m \geq 1 \end{cases}. \tag{8}$$

In the limit $\bar{n}\cdot k_i, \bar{n}\cdot k'_i \ll \bar{n}\cdot p$, the difference between $\bar{n}\cdot p$ and $\bar{n}\cdot p'$ in the spinors and Dirac matrices can be ignored. Accordingly, they can be simplified as follows

$$\bar{u}_n^{s'} \frac{\not{n}}{2} \frac{\not{n}}{2} \dots \frac{\not{n}}{2} \frac{\not{n}}{2} \frac{\not{n}}{2} u_n^s = \bar{u}_n^{s'} \frac{\not{n}}{2} u_n^s = (\bar{n}\cdot p) \delta^{s's}. \tag{9}$$

Besides, the transverse coordinates of the valence (anti)quark remain the same due to the delta function in the quark propagator.

Using the above results to simplify the rules in eq. (5) yields:

1. Feynman rules

$$\begin{aligned}
\text{External valence } q/\bar{q}: & \quad \xrightarrow{p} \cdot \mathbf{x} = 1 & \quad \xleftarrow{p} \cdot \mathbf{x} = 1 \\
\text{External gluon lines:} & \quad \xrightarrow{p} \cdot \mathbf{x} = \epsilon_\lambda(p) e^{i\mathbf{p}\cdot\mathbf{x}} & \quad \xleftarrow{p} \cdot \mathbf{x} = \epsilon_\lambda^*(p) e^{-i\mathbf{p}\cdot\mathbf{x}} \\
\text{Quark-gluon vertex:} & \quad \xrightarrow{\quad} \begin{array}{c} \text{gluon} \\ \text{c, } \mu \\ \text{c, } \mu \end{array} \xrightarrow{\quad} = -igt^c n^\mu \\
\text{Gluon propagator:} & \quad \xrightarrow{p} \cdot \mathbf{x}, \mu = \int \frac{d^2\mathbf{k}}{(2\pi)^2} \frac{-ig^{\mu\nu} e^{i\mathbf{k}\cdot(\mathbf{x}-\mathbf{y})}}{n \cdot p \bar{n} \cdot p - |\mathbf{k}|^2 + i\epsilon} \\
\text{valence quark propagator:} & \quad \xrightarrow{p} = \frac{i}{n \cdot p + i\bar{n} \cdot p \epsilon} \quad \xrightarrow{p} \text{ (cut)} = 1.
\end{aligned} \tag{10}$$

2. For an initial-state (anti)quark, insert a phase factor $e^{i\mathbf{p}\cdot\mathbf{x}}$ or $e^{-i\mathbf{p}\cdot\mathbf{x}}$ respectively in the amplitude or the conjugate amplitude. Here, \mathbf{p} and \mathbf{x} are respectively the transverse momentum and the transverse coordinates of the (anti)quark.

3. Impose the conservation of “+” momentum and spin across each (anti)quark line in the cut diagrams:

$$\Delta_+^{s's}(p, p', k) \equiv 2\bar{n} \cdot p \delta^{s's}(2\pi) \delta(\bar{n} \cdot p - \bar{n} \cdot k - \bar{n} \cdot p') \tag{11}$$

with k the total momentum of gluons.

4. Impose “-” momentum conservation for gluons hooked on the (anti)quark line respectively in the amplitude and the conjugate amplitude as long as the number of gluons is not zero. For a cut diagram with m and m' gluons in the amplitude and the conjugate amplitude respectively, one has

$$(2\pi) \delta^-(\sum_{i=1}^m n \cdot k_i) (2\pi) \delta^-(\sum_{i=1}^{m'} n \cdot k'_i) \tag{12}$$

with δ^- defined in eq. (8).

5. Integrate over transverse coordinates of (anti)quark lines and undetermined longitudinal momenta.

B. The impact-parameter dependent cross section for pion-pion collisions

Using the above Feynman rules, one can write down explicitly the expression for the impact-parameter dependent cross section in the collisions between baryons (color-singlet

triples) and/or mesons (color-singlet dipoles). Since the pion LFWFs are among the most studied ones [83], we focus on high-energy pion-pion collisions in the rest of this paper.

As detailed in sec. V A, the incoming pions are taken as valence $q\bar{q}$ states. Here, we need the LFWFs for mesons respectively moving along the two beam directions. Given one of the light-like vectors n^μ , the LFWF is expressed as

$$|\Psi_h(P)\rangle = \frac{1}{\sqrt{N_c}} \sum_{c=1}^{N_c} \sum_{s_q, s_{\bar{q}}, \xi} \int_{\mathbf{p}} \psi_{s_q s_{\bar{q}}/h}(\mathbf{p}, \xi) |p_q, c, s_q; p_{\bar{q}}, c, s_{\bar{q}}\rangle, \quad (13)$$

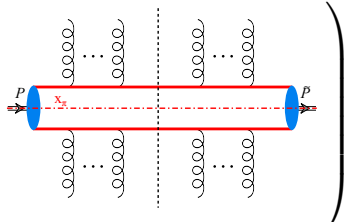
where s_q and $s_{\bar{q}}$ are the quark and antiquark spins respectively, c is the color index, the longitudinal momentum fraction $\xi \equiv \bar{n} \cdot p_q / \bar{n} \cdot P$ and in terms of the quark (antiquark) momentum p_q ($p_{\bar{q}}$) the pion transverse momentum \mathbf{P} and the relative momentum \mathbf{p} are respectively defined as

$$\mathbf{P} = \mathbf{p}_q + \mathbf{p}_{\bar{q}}, \quad \mathbf{p} = (1 - \xi)\mathbf{p}_q - \xi\mathbf{p}_{\bar{q}}. \quad (14)$$

Here, for brevity we have dropped some quantum numbers that are to be restored in sec. V A and used the following shorthand notation

$$\sum_{s, \bar{s}, \xi} \equiv \sum_{s_q, s_{\bar{q}}} \frac{1}{4\pi} \int_0^1 \frac{d\xi}{\xi(1-\xi)}, \quad \int_{\mathbf{p}} \equiv \int \frac{d^2\mathbf{p}}{(2\pi)^2}. \quad (15)$$

With pions taken as valence $q\bar{q}$ states, the evaluation of pion-pion cross sections is bogged down to that for the scattering of color-singlet dipoles. The impact-parameter dependent cross section in eq. (1) can be decomposed into two parts respectively associated with the two pions. Each part can be extracted from

$$S_\pi \equiv \int_{\mathbf{q}} \frac{e^{-i\mathbf{q}\cdot\mathbf{x}_\pi}}{\bar{n} \cdot P} \left(\text{cut diagram} \right), \quad (16)$$


where the cut diagram stands for the S -matrix element squared, \mathbf{x}_π is the pion transverse coordinates and $\mathbf{P} = -\tilde{\mathbf{P}} = \mathbf{q}/2$. Note that the number of gluons in the amplitude can be different from that in the conjugate amplitude since each gluon field can be either contracted with another one in the same S_π or in the other. Plugging the pion LFWF into the above

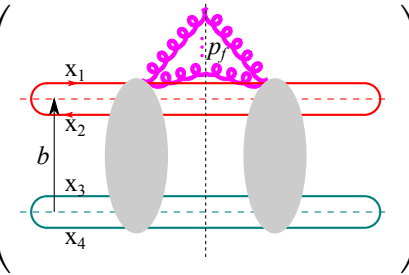
where the wave function in the mixed representation is given by Fourier transform:

$$\tilde{\psi}(\mathbf{r}, \xi) \equiv \int \frac{d^2\mathbf{p}}{(2\pi)^2} e^{i\mathbf{p}\cdot\mathbf{r}} \frac{\psi(\mathbf{p}, \xi)}{\sqrt{\xi(1-\xi)}}. \quad (22)$$

Finally, by removing the overall delta functions in the two S_π 's for $n = n_A$ and n_B and contracting all the gluon fields one has

$$\frac{d\sigma}{d^2\mathbf{b}dO} = \prod_{i=A,B} \int d^2\mathbf{r}_i \sum_{s_q^i, s_{\bar{q}}^i} \frac{1}{4\pi} \int_0^1 d\xi_i |\psi_{s_q^i s_{\bar{q}}^i/\sigma}(\mathbf{r}_i, \xi_i)|^2 \frac{d\hat{\sigma}}{d^2\mathbf{b}dO}, \quad (23)$$

where the dipole cross section at fixed impact parameter \mathbf{b} is defined as

$$\frac{d\hat{\sigma}}{d^2\mathbf{b}dO} \equiv \int \prod_f [d\Gamma_{p_f}] \delta(O - O(\{p_f\})) \frac{1}{N_c^2} \left(\begin{array}{c} \text{Diagram} \end{array} \right), \quad (24)$$


in which the transverse coordinates of the valence quarks and antiquarks of the two pions are given by

$$\begin{aligned} \mathbf{x}_1 &= \mathbf{x}_{A,q} = \mathbf{x}_A + (1 - \xi_A)\mathbf{r}_A, & \mathbf{x}_2 &= \mathbf{x}_{A,\bar{q}} = \mathbf{x}_A - \xi_A\mathbf{r}_A, \\ \mathbf{x}_3 &= \mathbf{x}_{B,q} = \mathbf{x}_B + (1 - \xi_B)\mathbf{r}_B, & \mathbf{x}_4 &= \mathbf{x}_{B,\bar{q}} = \mathbf{x}_B - \xi_B\mathbf{r}_B. \end{aligned} \quad (25)$$

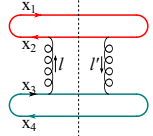
That is, the CM transverse coordinates of the two pions are identified with \mathbf{x}_A and \mathbf{x}_B respectively. As confirmed in the next section, the impact-parameter dependent cross section in eq. (24) is the same as that broadly used in parton saturation/small- x physics [94–97]. The above derivation hence confirms the generality of eq. (1) as the definition of the impact-parameter dependent cross section in quantum field theory.

III. FIXED-ORDER IMPACT-PARAMETER DEPENDENT CROSS SECTIONS

In this section we carry out detailed calculations of the impact-parameter dependent cross section and the azimuthal distribution for one gluon production in dipole-dipole collisions at leading order (LO).

A. The impact-parameter dependent cross section at LO

For the total impact-parameter dependent cross section, there are 16 cut diagrams corresponding to the 16 ways to connect the two dipoles with two gluon lines, each in the amplitude and the conjugate amplitude⁴. By using the Feynman rules in eq. (10), one has



$$\begin{aligned}
 &= \frac{g^4}{2} C_F N_c \int \frac{d^4 l}{(2\pi)^4} \frac{i n_A \cdot n_B}{l^2} e^{i l \cdot (\mathbf{x}_2 - \mathbf{x}_3)} 2\pi \delta(n_A \cdot l) 2\pi \delta(n_B \cdot l) \\
 &\quad \times \int \frac{d^4 l'}{(2\pi)^4} \frac{-i n_A \cdot n_B}{l'^2} e^{-i l' \cdot (\mathbf{x}_2 - \mathbf{x}_3)} 2\pi \delta(n_A \cdot l') 2\pi \delta(n_B \cdot l') \\
 &= \frac{g^4}{2} C_F N_c \int \frac{d^2 \mathbf{l}}{(2\pi)^2} \frac{e^{i \mathbf{l} \cdot (\mathbf{x}_2 - \mathbf{x}_3)}}{|\mathbf{l}|^2} \int \frac{d^4 \mathbf{l}'}{(2\pi)^2} \frac{e^{-i \mathbf{l}' \cdot (\mathbf{x}_2 - \mathbf{x}_3)}}{|\mathbf{l}'|^2}.
 \end{aligned} \tag{26}$$

And, including all possible hookings of the two gluons leads to

$$\frac{d\hat{\sigma}}{d^2 \mathbf{b}} = \frac{g^4 C_F}{2 N_c} \left| \int \frac{d^2 \mathbf{l}}{(2\pi)^2} \frac{1}{|\mathbf{l}|^2} \left(e^{i \mathbf{l} \cdot \mathbf{x}_1} - e^{i \mathbf{l} \cdot \mathbf{x}_2} \right) \left(e^{-i \mathbf{l} \cdot \mathbf{x}_3} - e^{-i \mathbf{l} \cdot \mathbf{x}_4} \right) \right|^2. \tag{27}$$

By using the integral

$$F_1(x, y) \equiv \mu^{2-d} \int \frac{d^d \mathbf{l}}{(2\pi)^d} \frac{e^{i \mathbf{l} \cdot \mathbf{x}}}{|\mathbf{l}|^2} = \frac{1}{4\pi} \frac{\Gamma(-\epsilon)}{(\pi r^2 \mu^2)^{-\epsilon}} = -\frac{1}{4\pi} \left[\frac{1}{\epsilon} + \gamma_E + \ln(\pi r^2 \mu^2) \right] \tag{28}$$

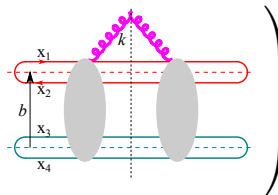
with $d = 2 - 2\epsilon$, one finally has

$$\begin{aligned}
 \frac{d\sigma}{d^2 \mathbf{b}} &= \frac{2\alpha_s^2 C_F}{N_c} \prod_{i=A,B} \int d^2 \mathbf{r}_i \sum_{s_q^i, s_{\bar{q}}^i} \frac{1}{4\pi} \int_0^1 \frac{d\xi_i}{\xi_i(1-\xi_i)} \\
 &\quad \times |\psi_{s_q^i s_{\bar{q}}^i/\sigma}(\mathbf{r}_i, \xi_i)|^2 \ln^2 \left(\frac{|\mathbf{x}_1 - \mathbf{x}_4| |\mathbf{x}_2 - \mathbf{x}_3|}{|\mathbf{x}_1 - \mathbf{x}_3| |\mathbf{x}_2 - \mathbf{x}_4|} \right).
 \end{aligned} \tag{29}$$

We, hence, confirm the known result in the literature (see, e.g., eq. (3.139) in ref. [93]).

B. Soft gluon production in dipole-dipole scattering

The impact-parameter dependent dipole cross section for radiating one gluon is given by



$$\frac{d\hat{\sigma}}{d^2 \mathbf{b} d\eta d^2 \mathbf{k}} = \frac{1}{2(2\pi)^3} \frac{1}{N_c^2} \left(\text{Diagram} \right) \tag{30}$$

⁴ Here, we only consider inelastic scattering in which the final-state $q\bar{q}$ pairs are not in color singlet.

The above dipole cross section respects the following symmetries. First, it is obviously invariant under $q \leftrightarrow \bar{q}$ in either dipole, i.e., $\mathbf{x}_1 \leftrightarrow \mathbf{x}_2$ or $\mathbf{x}_3 \leftrightarrow \mathbf{x}_4$. Second, it is invariant under $\mathbf{x}_1 \leftrightarrow \mathbf{x}_3$ and, simultaneously, $\mathbf{x}_2 \leftrightarrow \mathbf{x}_4$, as required by gauge invariance. This is not evident on the amplitude level since the relevant diagrams admit the interpretation as soft gluon radiation by the emitters of valence q and \bar{q} of pion A in $n_B \cdot A = 0$ gauge. In $n_A \cdot A = 0$ gauge, the dipole cross section is, instead, given by that in $n_B \cdot A = 0$ gauge with $\mathbf{x}_1 \leftrightarrow \mathbf{x}_3$ and $\mathbf{x}_2 \leftrightarrow \mathbf{x}_4$. The equivalence of these two results can be straightforwardly verified by using the following relation

$$\begin{aligned} & \frac{2}{|\mathbf{l}|^2 |\mathbf{l}'|^2} \left(|\mathbf{k}|^2 - \frac{\mathbf{k} \cdot \mathbf{l}}{|\mathbf{k} - \mathbf{l}|^2} \right) \cdot \left(\frac{\mathbf{k}}{|\mathbf{k}|^2} - \frac{\mathbf{k} - \mathbf{l}'}{|\mathbf{k} - \mathbf{l}'|^2} \right) \\ &= \frac{1}{|\mathbf{l}|^2 |\mathbf{k}|^2 |\mathbf{l}' - \mathbf{k}|^2} + \frac{1}{|\mathbf{l}'|^2 |\mathbf{k}|^2 |\mathbf{l} - \mathbf{k}|^2} - \frac{|\mathbf{l} - \mathbf{l}'|^2}{|\mathbf{l}|^2 |\mathbf{l}'|^2 |\mathbf{l} - \mathbf{k}|^2 |\mathbf{l}' - \mathbf{k}|^2}. \end{aligned} \quad (36)$$

C. Evaluation of the dipole cross section for soft gluon production

Let us write the dipole cross section eq. (35) in the following form

$$\frac{d\hat{\sigma}}{d^2\mathbf{b}d\eta d^2\mathbf{k}} = 8\alpha_s^3 C_F |\mathbf{J}(\{\mathbf{x}_i\})|^2 \quad (37)$$

with

$$\mathbf{J}(\{\mathbf{x}_i\}) \equiv \int \frac{d^2\mathbf{l}}{(2\pi)^2} \frac{1}{|\mathbf{l}|^2} (e^{-i\mathbf{l} \cdot \mathbf{x}_3} - e^{-i\mathbf{l} \cdot \mathbf{x}_4}) \left(\frac{\mathbf{k}}{|\mathbf{k}|^2} - \frac{\mathbf{k} - \mathbf{l}}{|\mathbf{k} - \mathbf{l}|^2} \right) [e^{i(\mathbf{l} - \mathbf{k}) \cdot \mathbf{x}_1} - e^{i(\mathbf{l} - \mathbf{k}) \cdot \mathbf{x}_2}]. \quad (38)$$

In terms of the integrals

$$F_1(x, y) \equiv \int \frac{d^2\mathbf{l}}{(2\pi)^2} \frac{e^{i\mathbf{l} \cdot \mathbf{x}}}{|\mathbf{l}|^2}, \quad F_2(x, y) \equiv \int \frac{d^2\mathbf{l}}{(2\pi)^2} \frac{e^{i\mathbf{l} \cdot \mathbf{x}}}{|\mathbf{l}|^2 |\mathbf{k} - \mathbf{l}|^2}, \quad (39)$$

\mathbf{J} can be expressed as

$$\begin{aligned} \mathbf{J}(\{\mathbf{x}_i\}) &= \frac{\mathbf{k}}{|\mathbf{k}|^2} \left\{ [F_1(\mathbf{x}_{13}) - F_1(\mathbf{x}_{14})] e^{-i\mathbf{k} \cdot \mathbf{x}_1} - [F_1(\mathbf{x}_{23}) - F_1(\mathbf{x}_{24})] e^{-i\mathbf{k} \cdot \mathbf{x}_2} \right\} \\ &\quad - e^{-i\mathbf{k} \cdot \mathbf{x}_1} (\mathbf{k} + i\nabla) [F_2(\mathbf{x}_{13}) - F_2(\mathbf{x}_{14})] + e^{-i\mathbf{k} \cdot \mathbf{x}_2} (\mathbf{k} + i\nabla) [F_2(\mathbf{x}_{23}) - F_2(\mathbf{x}_{24})], \end{aligned} \quad (40)$$

where $\mathbf{x}_{ij} \equiv \mathbf{x}_i - \mathbf{x}_j$, and $\nabla = (\partial_x, \partial_y)$ acts on the two-dimensional coordinate space.

Both F_1 and F_2 are singular while \mathbf{J} is finite. One can further single out the divergent piece of F_2 by using the following relation

$$F_2 = \frac{1 + e^{i\mathbf{k} \cdot \mathbf{x}}}{|\mathbf{k}|^2} F_1 - \frac{2}{|\mathbf{k}|^2} F_3, \quad (41)$$

where the finite integral F_3 is defined as

$$F_3(\mathbf{x}) \equiv \int \frac{d^2\mathbf{l}}{(2\pi)^2} e^{i\mathbf{l}\cdot\mathbf{x}} \frac{\mathbf{l}\cdot(\mathbf{l}-\mathbf{k})}{|\mathbf{l}|^2|\mathbf{k}-\mathbf{l}|^2}. \quad (42)$$

F_1 , regularized by dimensional regularization, is given in eq. (28) and here we only need to evaluate F_3 . Let us choose a frame with the basis vectors given by

$$\mathbf{e}_1 = \frac{\mathbf{k} - \frac{\mathbf{k}\cdot\mathbf{x}}{r}\frac{\mathbf{x}}{r}}{\left|\mathbf{k} - \frac{\mathbf{k}\cdot\mathbf{x}}{r}\frac{\mathbf{x}}{r}\right|}, \quad \mathbf{e}_2 = \frac{\mathbf{x}}{r}. \quad (43)$$

In this frame, one has

$$\mathbf{x} = (x_1, x_2) = (0, r), \quad \mathbf{k} = (k_1, k_2) = \left(\left| \mathbf{k} - \frac{\mathbf{k}\cdot\mathbf{x}}{r}\frac{\mathbf{x}}{r} \right|, \frac{\mathbf{k}\cdot\mathbf{x}}{r} \right), \quad (44)$$

and the integration over l_1 can be easily carried out by using the residue theorem with the poles given by

$$l_1 = \pm il_2, \quad k_1 \pm i(l_2 - k_2). \quad (45)$$

Then, making a Fourier transform of l_2 yields

$$\begin{aligned} F_3(r, \mathbf{k}) = & \frac{1}{8\pi} e^{-\frac{1}{2}r(k_1 - ik_2)} \left\{ -e^{k_1 r} \left[\text{Ci} \left(\frac{1}{2}(ik_1 - k_2)r \right) + \text{Ci} \left(\frac{1}{2}(-ik_1 - k_2)r \right) \right. \right. \\ & - i\text{Si} \left(\frac{1}{2}(-ik_1 + k_2)r \right) + i\text{Si} \left(\frac{1}{2}(ik_1 + k_2)r \right) \left. \right] - \text{Ci} \left(\frac{1}{2}(k_2 - ik_1)r \right) \\ & \left. - \text{Ci} \left(\frac{1}{2}(ik_1 + k_2)r \right) - i\text{Si} \left(\frac{1}{2}(-ik_1 + k_2)r \right) + i\text{Si} \left(\frac{1}{2}(ik_1 + k_2)r \right) \right\}, \quad (46) \end{aligned}$$

where Ci and Si are the cosine and sine integral functions respectively.

The above expression for F_3 , obtained by assuming two independent bases, breaks down when $\mathbf{k} \parallel \mathbf{x}$ or, equivalently, $\mathbf{e}_1 \parallel \mathbf{e}_2$. In general cases the expression of \mathbf{J} can be shown to reduce to the following form

$$\mathbf{J} = \mathbf{A}(\mathbf{x}_{13})e^{-i\mathbf{k}\cdot\mathbf{x}_1} - \mathbf{A}(\mathbf{x}_{14})e^{-i\mathbf{k}\cdot\mathbf{x}_1} - \mathbf{A}(\mathbf{x}_{23})e^{-i\mathbf{k}\cdot\mathbf{x}_2} + \mathbf{A}(\mathbf{x}_{24})e^{-i\mathbf{k}\cdot\mathbf{x}_2}, \quad (47)$$

where

$$\mathbf{A}(\mathbf{x}) = \frac{\mathbf{k}}{|\mathbf{k}|^2} F_1(\mathbf{x})e^{i\mathbf{k}\cdot\mathbf{x}} + \frac{1}{|\mathbf{k}|^2} \left[-2\mathbf{k}(-i\mathbf{k}\cdot\nabla) + |\mathbf{k}|^2(-i\nabla) \right] F_2(\mathbf{x}). \quad (48)$$

After some algebra, we arrive at the following expression

$$\mathbf{A}(\mathbf{x}) = -\frac{\mathbf{k}}{|\mathbf{k}|^2} (I_0 + I_1) + \frac{1}{|\mathbf{k}|^2} \left[2\mathbf{k}(\mathbf{k}\cdot\mathbf{x}) - |\mathbf{k}|^2\mathbf{x} \right] (I_2 + I_3), \quad (49)$$

with

$$I_0 = \frac{e^{i\chi\rho}}{4\pi} \left[\text{Ci}(|\rho|\chi) - i \text{Si}(\rho\chi) + \log \frac{\chi}{4|\rho|} + \gamma_E \right], \quad (50a)$$

$$I_1 = \frac{\chi}{4\pi} \int_0^1 d\alpha \alpha \frac{e^{i\alpha\rho\chi}}{\sqrt{\alpha(1-\alpha)}} \left\{ K_1 \left(\chi\sqrt{\alpha(1-\alpha)} \right) - \frac{1}{\chi\sqrt{\alpha(1-\alpha)}} \right\}, \quad (50b)$$

$$I_2 = -\frac{i}{4\pi} \int_0^1 d\alpha e^{i\alpha\rho\chi} \left\{ K_0 \left(\chi\sqrt{\alpha(1-\alpha)} \right) + \log \chi \right\}, \quad (50c)$$

$$I_3 = -\frac{1}{4\pi} (1 - e^{i\rho\chi}) \frac{\log \chi}{\rho\chi}. \quad (50d)$$

Here, the I 's are functions of two dimensionless variables $\chi \equiv |\mathbf{k}||\mathbf{x}|$ and $\rho \equiv \cos(\phi - \theta_x)$ with $\phi \equiv \arg \mathbf{k}$ the azimuthal angle of the gluon momentum and θ_x the azimuthal angle of \mathbf{x} , such that $\mathbf{k} \cdot \mathbf{x} = \chi\rho$, and K_n is the Bessel function. By numerically evaluating the above integrals, we have checked that the above two expressions for \mathbf{J} , eqs. (40) and (47), agree with each other for $\mathbf{k} \not\parallel \mathbf{x}$. Moreover, they are also found to yield the same v_n (within numerical errors) due to the fact that the measure for the subspace of dipole orientations corresponding to $\mathbf{k} \parallel \mathbf{x}$ is zero when one integrates over the azimuthal angles.

In the following discussions the impact parameter is taken to be aligned with the positive x -axis and so are the pion transverse positions during the collision:

$$\mathbf{x}_A = (b/2, 0), \quad \mathbf{x}_B = (-b/2, 0), \quad \text{and} \quad \mathbf{b} = (b, 0). \quad (51)$$

The dipole cross section for an arbitrary dipole orientation can be easily obtained by translations and rotations in the transverse plane: First, one can translate the whole collision system, moving the midpoint of its impact parameter to the origin as it is invariant under translations. Then, the dipole cross section is obtained by rotating the corresponding one for the above dipole orientation by a proper angle $\Delta\phi$ according to

$$\left. \frac{d\hat{\sigma}}{d\phi}(\phi) \right|_{\text{rotated by } \Delta\phi} = \frac{d\hat{\sigma}}{d\phi}(\phi - \Delta\phi). \quad (52)$$

Note also that under reflections over x -axis and y -axis, it transforms respectively as

$$\left. \frac{d\hat{\sigma}}{d\phi}(\phi) \right|_{y \rightarrow -y} = \frac{d\hat{\sigma}}{d\phi}(-\phi), \quad \left. \frac{d\hat{\sigma}}{d\phi}(\phi) \right|_{x \rightarrow -x} = \frac{d\hat{\sigma}}{d\phi}(\pi - \phi). \quad (53)$$

D. Momentum anisotropies in soft gluon production

The azimuthal flow coefficients v_n and their associated flow angles ψ_n are defined as

$$\frac{d\sigma}{d\phi} = \frac{\sigma}{2\pi} \left[1 + 2 \sum_n v_n \cos(n(\phi - \psi_n)) \right], \quad (54)$$

such that $v_n > 0$ ⁵. Here, the dependence of σ on \mathbf{b}, η and k_T are omitted for brevity. To facilitate our discussions below, we define two-dimensional flow coefficients \mathbf{v}_n with their components respectively given by

$$v_n^x = \frac{1}{\sigma} \int_0^{2\pi} d\phi \frac{d\sigma}{d\phi} \cos(n\phi), \quad v_n^y = \frac{1}{\sigma} \int_0^{2\pi} d\phi \frac{d\sigma}{d\phi} \sin(n\phi). \quad (55)$$

That is,

$$\frac{d\sigma}{d\phi} = \frac{\sigma}{2\pi} \left[1 + 2 \sum_n (v_n^x \cos(n\phi) + v_n^y \sin(n\phi)) \right]. \quad (56)$$

And one has, accordingly,

$$v_n = |\mathbf{v}_n|, \quad \psi_n = \frac{1}{n} \phi_{\mathbf{v}_n} \quad (57)$$

with $\phi_{\mathbf{v}_n}$ the azimuthal angle of \mathbf{v}_n around the x -axis.

IV. MOMENTUM ANISOTROPIES IN DIPOLE-DIPOLE SCATTERING

In this section, we study transverse momentum anisotropies, mainly v_2 , of soft gluon production in dipole-dipole scattering. We first study the k_T -dependence of v_2 and evaluate it analytically both at low and high k_T . Then, we calculate v_2 for the intermediate k_T regime numerically with the afore-derived exact expression and investigate the correlation between momentum anisotropies and dipole orientations.

A. The low k_T limit

In the limit $k_T \rightarrow 0$ when the de Broglie wavelength of the produced gluon is larger than the dipole sizes and the impact parameter, momentum anisotropies are expected to vanish.

⁵ As discussed in the following sections, ψ_n is not necessarily equal to the reaction plane angle in the corresponding classical collision geometry.

This can be explicitly checked from eq. (35):

$$\frac{d\hat{\sigma}}{d^2\mathbf{b}d\eta d^2\mathbf{k}} \rightarrow \frac{\alpha_s N_c}{\pi^2} \frac{1}{|\mathbf{k}|^2} \frac{d\hat{\sigma}}{d^2\mathbf{b}} \quad \text{as } k_T \rightarrow 0, \quad (58)$$

which shows explicitly $v_n \rightarrow 0$ as $k_T \rightarrow 0$. Here, the LO total dipole cross section is given in eq. (27).

Let us evaluate the behavior of \mathbf{v}_2 at low k_T via the expressions of $|\mathbf{J}|^2$. The small k_T limit of $|\mathbf{J}|^2$ can be obtained by directly expanding its components I_0, I_1, I_2 and I_3 [see eq. (50)] at $\chi = 0$; recall that $\chi = |\mathbf{k}||\mathbf{x}|$. The angular dependence resides in $\rho [= \cos(\theta_x - \phi)]$, and here we keep $|\mathbf{J}|^2$ up to $\mathcal{O}(\chi^0)$, the lowest order in χ containing ρ . The corresponding expansions of I 's are

$$\begin{aligned} \lim_{\chi \rightarrow 0} I_0 &= \frac{1}{4\pi} \left(\log \frac{\chi^2}{4} + 2\gamma_E \right) + \frac{i\rho\chi}{4\pi} \left(\log \frac{\chi^2}{4} + 2\gamma_E - 1 \right) \\ &\quad - \frac{\rho^2\chi^2}{8\pi} \left(\log \frac{\chi^2}{4} + 2\gamma_E - \frac{3}{2} \right) + \mathcal{O}(\chi^3), \end{aligned} \quad (59a)$$

$$\lim_{\chi \rightarrow 0} I_1 = \frac{\chi^2}{32\pi} \left(\log \frac{\chi^2}{4} + 2\gamma_E - 3 \right) + \mathcal{O}(\chi^3), \quad (59b)$$

$$\lim_{\chi \rightarrow 0} I_2 + I_3 = -\frac{1}{16\pi} (-2i + \rho\chi) \left(\log \frac{\chi^2}{4} + 2\gamma_E - 2 \right) + \mathcal{O}(\chi^2). \quad (59c)$$

The expansion for $\mathbf{A}(\mathbf{x})$ follows as

$$\begin{aligned} \lim_{k_T \rightarrow 0} \mathbf{A}(\mathbf{x}) &= -\frac{\mathbf{k}}{|\mathbf{k}|^2} \frac{1}{4\pi} \left(\log \frac{|\mathbf{k}|^2|\mathbf{x}|^2}{4} + 2\gamma_E \right) + \frac{\mathbf{x}}{16\pi} (\mathbf{k} \cdot \mathbf{x}) \left(\log \frac{|\mathbf{k}|^2|\mathbf{x}|^2}{4} + 2\gamma_E - 2 \right) \\ &\quad + \frac{\mathbf{k}}{|\mathbf{k}|^2} \left[\frac{(\mathbf{k} \cdot \mathbf{x})^2}{16\pi} - \frac{\mathbf{k}^2\mathbf{x}^2}{32\pi} \left(\log \frac{\mathbf{k}^2\mathbf{x}^2}{4} + 2\gamma_E - 3 \right) \right] \\ &\quad - i \frac{\mathbf{k}}{|\mathbf{k}|^2} \frac{(\mathbf{k} \cdot \mathbf{x})}{4\pi} - i \frac{\mathbf{x}}{8\pi} \left(\log \frac{\mathbf{k}^2|\mathbf{x}|^2}{4} + 2\gamma_E - 2 \right) + \mathcal{O}(|\mathbf{k}|^2). \end{aligned} \quad (60)$$

The resulting $|\mathbf{J}|^2$ has the following format

$$\lim_{k_T \rightarrow 0} |\mathbf{J}|^2 = \frac{1}{|\mathbf{k}|^2} \left[B_0 + |\mathbf{k}|^2 \sum_{i,j=1}^4 D_{ij} \cos(\theta_i - \phi) \cos(\theta_j - \phi) \right] + \mathcal{O}(|\mathbf{k}|), \quad (61)$$

in which $\theta_i = \arg \mathbf{x}_i$ and the coefficients B_0 and D_{ij} do not depend on the angle $\phi (= \arg \mathbf{k})$:

$$\begin{aligned} B_0 &= \frac{1}{16\pi^2} \left(\log \frac{|\mathbf{x}_{13}|^2 |\mathbf{x}_{24}|^2}{|\mathbf{x}_{14}|^2 |\mathbf{x}_{23}|^2} \right)^2, & D_{ij} &= -\frac{1}{32\pi^2} \log \frac{|\mathbf{x}_{13}|^2 |\mathbf{x}_{24}|^2}{|\mathbf{x}_{14}|^2 |\mathbf{x}_{23}|^2} |\mathbf{x}_i| |\mathbf{x}_j| f_{ij}, \\ f_{ij} &= \begin{cases} (-1)^{i+1} \log \frac{|\mathbf{x}_{i,l(i)}|^2}{|\mathbf{x}_{i,l(i)+1}|^2}, & \text{if } i = j \\ (-1)^{i-j} \left[1 - \log \frac{|\mathbf{k}|^2 |\mathbf{x}_{ij}|^2}{4} \right], & \text{if } i \neq j \end{cases}, & l(i) &\equiv \begin{cases} 3, & \text{if } i = 1, 2 \\ 1, & \text{if } i = 3, 4 \end{cases}. \end{aligned}$$

Integrating over ϕ , one obtains

$$\lim_{k_T \rightarrow 0} \int_0^{2\pi} d\phi |\mathbf{J}|^2 = \frac{2\pi}{|\mathbf{k}|^2} \left[B_0 + \frac{|\mathbf{k}|^2}{2} \sum_{i,j=1}^4 D_{ij} \cos(\theta_i - \theta_j) \right] + \mathcal{O}(|\mathbf{k}|), \quad (62a)$$

$$\lim_{k_T \rightarrow 0} \int_0^{2\pi} d\phi |\mathbf{J}|^2 \cos(2\phi) = \frac{\pi}{2} \sum_{i,j=1}^4 D_{ij} \cos(\theta_i + \theta_j) + \mathcal{O}(|\mathbf{k}|). \quad (62b)$$

Note that here we are evaluating v_2^x as defined in eq. (55), and the calculation of v_2^y is similar. Besides, for the reason that will be explained later, v_2^y vanishes for azimuthally-integrated dipoles (i.e., as in the pion-pion case) and thus $v_2 = |v_2^x|$. It follows that v_2 scales as k_T^2 at small k_T :

$$\lim_{k_T \rightarrow 0} v_2 = \frac{\sum_{i,j=1}^4 D_{ij}}{4B_0} \cos(\theta_i + \theta_j) |\mathbf{k}|^2 + \mathcal{O}(|\mathbf{k}|^3). \quad (63)$$

B. The high k_T limit

At high k_T when the gluon has a de Broglie wavelength much shorter than the dipole sizes and the impact parameter, one may expect that the azimuthal distribution of the gluon is only sensitive to its emitter (q or \bar{q}) and, hence, isotropic. This is also needed in order to justify that the production of high- k_T partons can be sufficiently described by the single parton distribution functions or the thickness beam functions of pions, which are rotationally symmetric in the transverse plane [92].

In order to evaluate the behavior of \mathbf{v}_2 at large k_T via $|\mathbf{J}|^2$, we use the expressions of F_1 and F_2 and expand $|\mathbf{J}|^2$ at $1/|\mathbf{k}| = 0$. We apply the method of regions on F_2 , by noting two dominant regions: $\mathbf{l} \sim \mathbf{k}$ and $\mathbf{l} \sim \mathbf{0}$. These two regions are well-separated in the large k_T limit, and one obtains

$$\begin{aligned} \lim_{k_T \rightarrow \infty} F_2(\mathbf{x}) &= \mu^{2\epsilon} \int \frac{d^d l}{(2\pi)^d} \frac{e^{i\mathbf{l}\cdot\mathbf{x}}}{|\mathbf{l}|^2} \left[\frac{1}{|\mathbf{k}|^2} + \frac{2\mathbf{k}\cdot\mathbf{l}}{|\mathbf{k}|^4} \right] + \mu^{2\epsilon} \int \frac{d^d l}{(2\pi)^d} \frac{e^{i\mathbf{l}\cdot\mathbf{x}}}{|\mathbf{l}-\mathbf{k}|^2} \left[\frac{3}{|\mathbf{k}|^2} - \frac{2\mathbf{k}\cdot\mathbf{l}}{|\mathbf{k}|^4} \right] \\ &\quad + \mathcal{O}\left(\frac{1}{|\mathbf{k}|^4}\right) \\ &= -\frac{1+e^{i\mathbf{k}\cdot\mathbf{x}}}{4\pi|\mathbf{k}|^2} \left[\frac{1}{\epsilon} + \log(|\mathbf{x}|^2 \mu^2) + \gamma_E + \log \pi \right] + \frac{1-e^{i\mathbf{k}\cdot\mathbf{x}}}{\pi|\mathbf{k}|^4} \frac{i\mathbf{k}\cdot\mathbf{x}}{|\mathbf{x}|^2} + \mathcal{O}\left(\frac{1}{|\mathbf{k}|^4}\right), \end{aligned} \quad (64)$$

where we have applied the expression of F_1 in eq. (28). The expansion for $\mathbf{A}(\mathbf{x})$ follows as

$$\lim_{k_T \rightarrow \infty} \mathbf{A}(\mathbf{x}) = -\frac{i\mathbf{k}}{\pi|\mathbf{k}|^4|\mathbf{x}|^2} (\mathbf{k}\cdot\mathbf{x}) + \frac{i\mathbf{x}}{2\pi|\mathbf{k}|^2|\mathbf{x}|^2} (1+e^{i\mathbf{k}\cdot\mathbf{x}}) + \mathcal{O}\left(\frac{1}{|\mathbf{k}|^3}\right). \quad (65)$$

The resulting $|\mathbf{J}|^2$ is in the following format

$$\lim_{k_T \rightarrow \infty} |\mathbf{J}|^2 = \frac{1}{|\mathbf{k}|^4} \left\{ B_1 + \left[\sum_{\substack{m,n=1 \\ m \neq n}}^4 f_{mn} + \sum_{\substack{n=1,2 \\ m=3,4}} g_{mn} \cos(2\phi) + \sum_{\substack{n=1,2 \\ m=3,4}} h_{mn} \sin(2\phi) \right] \right. \\ \left. \cos [|\mathbf{k}| |\mathbf{x}_m| \cos(\theta_m - \phi) - |\mathbf{k}| |\mathbf{x}_n| \cos(\theta_n - \phi)] \right\} + \mathcal{O} \left(\frac{1}{|\mathbf{k}|^6} \right), \quad (66)$$

in which the coefficients $B_1, f_{mn}, g_{mn}, h_{mn}$ do not depend on ϕ :

$$\mathbf{Q}_1 \equiv -\frac{\mathbf{x}_{13}}{x_{13}^2} + \frac{\mathbf{x}_{14}}{x_{14}^2}, \quad \mathbf{Q}_2 \equiv \frac{\mathbf{x}_{23}}{x_{23}^2} - \frac{\mathbf{x}_{24}}{x_{24}^2}, \quad \mathbf{Q}_3 \equiv -\frac{\mathbf{x}_{13}}{x_{13}^2} + \frac{\mathbf{x}_{23}}{x_{23}^2}, \quad \mathbf{Q}_4 \equiv \frac{\mathbf{x}_{14}}{x_{14}^2} - \frac{\mathbf{x}_{24}}{x_{24}^2}, \\ B_1 \equiv \frac{1}{4\pi^2} \sum_{i=1}^4 |\mathbf{Q}_i|^2, \quad f_{mn} \equiv \frac{1}{4\pi^2} \mathbf{Q}_m \cdot \mathbf{Q}_n, \quad \theta_{Q_n} = \arg \mathbf{Q}_n, \\ g_{mn} \equiv -\frac{1}{2\pi^2} |\mathbf{Q}_m| |\mathbf{Q}_n| \cos(\theta_{Q_m} + \theta_{Q_n}), \quad h_{mn} \equiv -\frac{1}{2\pi^2} |\mathbf{Q}_m| |\mathbf{Q}_n| \sin(\theta_{Q_m} + \theta_{Q_n}).$$

Integrating over ϕ , one obtains

$$\lim_{k_T \rightarrow \infty} \int_0^{2\pi} d\phi |\mathbf{J}|^2 = \frac{2\pi}{|\mathbf{k}|^4} B_1 + \frac{2\pi}{|\mathbf{k}|^4} \left[\sum_{\substack{m,n=1 \\ m \neq n}}^4 f_{mn} J_0[|\mathbf{k}| \bar{x}_{mn}] - \sum_{\substack{n=1,2 \\ m=3,4}} g_{mn} J_2[|\mathbf{k}| \bar{x}_{mn}] \right] \\ + \mathcal{O} \left(\frac{1}{|\mathbf{k}|^6} \right), \quad (67a)$$

$$\lim_{k_T \rightarrow \infty} \int_0^{2\pi} d\phi |\mathbf{J}|^2 \cos(2\phi) = \frac{2\pi}{|\mathbf{k}|^4} \left[-\sum_{\substack{m,n=1 \\ m \neq n}}^4 f_{mn} J_2[|\mathbf{k}| \bar{x}_{mn}] + \sum_{\substack{n=1,2 \\ m=3,4}} g_{mn} J_0[|\mathbf{k}| \bar{x}_{mn}] \right] \\ + \mathcal{O} \left(\frac{1}{|\mathbf{k}|^5} \right), \quad (67b)$$

in which $\bar{x}_{mn} \equiv x_m^x + x_m^y - x_n^x - x_n^y$, and J_t is the t -th Bessel J function. It follows that v_2 scales as $1/\sqrt{k_T}$ at large k_T :

$$\lim_{k_T \rightarrow \infty} v_2 = \frac{\left[-\sum_{\substack{m,n=1 \\ m \neq n}}^4 f_{mn} J_2[|\mathbf{k}| \bar{x}_{mn}] + \sum_{\substack{n=1,2 \\ m=3,4}} g_{mn} J_0[|\mathbf{k}| \bar{x}_{mn}] \right] + \mathcal{O}(1/|\mathbf{k}|)}{B_1 + \left[\sum_{\substack{m,n=1 \\ m \neq n}}^4 f_{mn} J_0[|\mathbf{k}| \bar{x}_{mn}] - \sum_{\substack{n=1,2 \\ m=3,4}} g_{mn} J_2[|\mathbf{k}| \bar{x}_{mn}] \right] + \mathcal{O}(1/|\mathbf{k}|^2)} \\ = \frac{1}{B_1} \sqrt{\frac{2}{\pi|\mathbf{k}|}} \left[\sum_{\substack{m,n=1 \\ m \neq n}}^4 \frac{f_{mn}}{\sqrt{\bar{x}_{mn}}} \cos(|\mathbf{k}| \bar{x}_{mn} - \frac{\pi}{4}) + \sum_{\substack{n=1,2 \\ m=3,4}} \frac{g_{mn}}{\sqrt{\bar{x}_{mn}}} \cos(|\mathbf{k}| \bar{x}_{mn} - \frac{\pi}{4}) \right] \\ + \mathcal{O} \left(\frac{1}{|\mathbf{k}|} \right). \quad (68)$$

Strictly speaking, this result is valid at large $k_T \bar{x}_{mn}$ instead of large k_T . One can see that the large- k_T expression of $|\mathbf{J}|^2$ diverges at $\bar{x}_{mn} = 0$ (e.g., $x_{13} = 0$), whereas the full expression in sec. III C is finite.

C. The intermediate k_T -dependence

In this subsection we study the transition of v_2 from the quadratic growth at low k_T to the $1/\sqrt{k_T}$ suppression at high k_T . For such an intermediate range of k_T , we use the full result of the dipole cross section in sec. III C to evaluate v_2 numerically. Since v_2 in pion-pion collisions results from the superposition of gluons emitted off all the possible dipole orientations weighted by the pion wave functions, below we investigate the dependence of v_2 on dipole orientations, characterized by b , r_A , ϕ_A , r_B and ϕ_B with r_i and ϕ_i respectively the azimuthal angle and the modulus of \mathbf{r}_i . As motivated by the fact that the valence q or \bar{q} typically carries half of the “+” momentum of its parent pion, we take $\xi_A = \xi_B = 1/2$ in the following discussions.

1. v_2 for “typical” dipole orientations with $\phi_A = \phi_B = \pi/2$

As shown in the following sections, some main qualitative features of v_2 for the dipole configurations with $(\phi_A, \phi_B) = (\pi/2, \pi/2)$ survive the integration over the LFWFs in pion-pion collisions. In order to discuss such qualitative features, let us first fix b (along the x -axis according to eq. (51)) and vary the dipole sizes $r_A = r_B \equiv d_{dp}$ with both dipole azimuthal angles fixed to be $\pi/2$. For such dipole configurations one has $\frac{d\sigma}{d\phi}(\phi) = \frac{d\sigma}{d\phi}(-\phi)$ according to eq. (53) and, as a result, v_2^y vanishes.

Figure 1 shows the dependence of v_2^x on k_T for different dipole sizes: $d_{dp} = 0.1b, b$ and $2b$. For all these dipole sizes, v_2^x is observed to grow quadratically in k_T at small k_T while it damps and oscillates at large k_T . In the shown range of $k_T \leq 30b^{-1}$, the curves for $d_{dp} = b$ and $2b$ can be fairly approximated by our analytic results both at low and high k_T while the curve for $d_{dp} = 0.1b$ approaches to the asymptotic high- k_T behavior only at $k_T > 30b^{-1}$ when $k_T \bar{x}_{mn}$, as in eq. (68), is sufficiently large.

At intermediate k_T , Fig. 1 shows a qualitative difference between the more central ($d_{dp} = 2b$) and the more peripheral ($d_{dp} = b$ and $0.1b$) collisions. At $k_T \sim 1/b$, all the curves of $v_2 =$

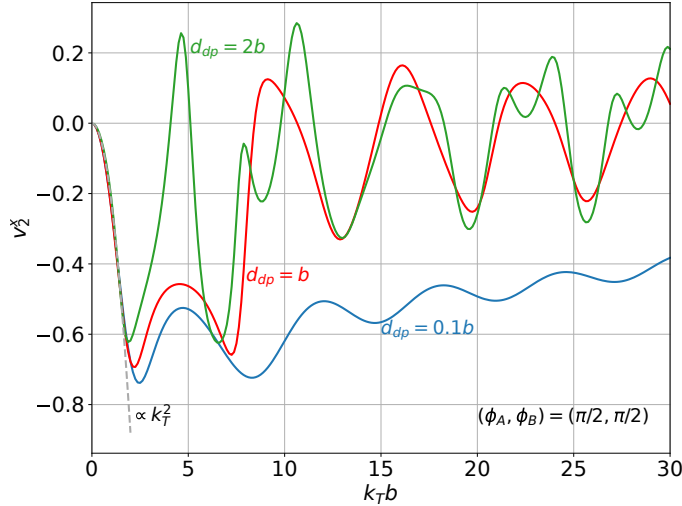


FIG. 1. v_2^x as a function of k_T at b for different dipole sizes with $(\phi_A, \phi_B) = (\pi/2, \pi/2)$. Here, both dipoles have the same size d_{dp} .

$|v_2^x|$ start to deviate from the quadratic growth and develop their first peak (corresponding to the first minimum of v_2^x). Then, as k_T increases, v_2^x for $d_{dp} = 2b$ changes its sign after passing its first minimum. In contrast, there is no sign change in the curves for $d_{dp} = b$ or $d_{dp} = 0.1b$ before they develop their second minimum; and no sign change is observed for $d_{dp} = 0.1b$ in the shown range of k_T up to $30b^{-1}$. Such a sign change after the first minimum of v_2^x is found to exist for $d_{dp} \gtrsim 1.5b$.

2. v_2 for different dipole azimuthal angles

Let us further investigate the dependence of v_2 on (ϕ_A, ϕ_B) . The dipole sizes r_A and r_B , denoted by d_{dp} , are now kept fixed (it could be estimated as the hadron size or the charge radius defined in the next section). As we are only interested in collisions dominated by the strong interaction, below we investigate in detail two sets of dipole orientations with $b = 0.5d_{dp}$ and $b = d_{dp}$ respectively.

Since the pion wave function squared respects rotational symmetry (in the transverse plane), we first study the net effect of integrating over ϕ_A and ϕ_B on v_2 . In this case the contributions to v_n^y from (ϕ_A, ϕ_B) and $(-\phi_A, -\phi_B)$ cancel due to reflection symmetry over the x -axis and, accordingly, the (ϕ_A, ϕ_B) -integrated $v_n^y = 0$. The results of v_2^x for

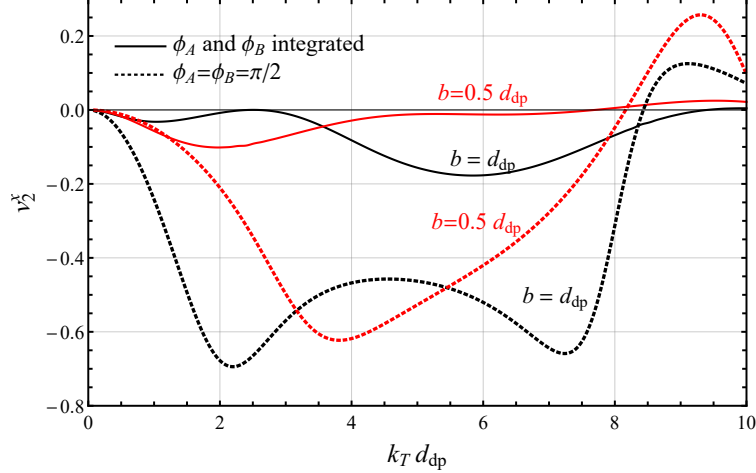


FIG. 2. The (ϕ_A, ϕ_B) -integrated v_2^x as a function of k_T at $b = 0.5d_{dp}$ and $b = d_{dp}$. To facilitate comparison, the results (dashed) for $(\phi_A, \phi_B) = (\pi/2, \pi/2)$ in Fig. 1 are replotted as a function of $k_T d_{dp}$ in this figure.

$b = 0.5d_{dp}$ and $b = d_{dp}$, in comparison with those for the typical dipole orientations with $(\phi_A, \phi_B) = (\pi/2, \pi/2)$, are shown in Fig. 2. The main qualitative features observed for $(\phi_A, \phi_B) = (\pi/2, \pi/2)$ survive: the curve for $b = 0.5d_{dp}$ only develops one (global) minimum while the other one for $b = d_{dp}$ has two minima before entering the suppression region at high k_T . Quantitatively, the absolute values of the minima are smaller and their locations are shifted to lower k_T compared to those for $(\phi_A, \phi_B) = (\pi/2, \pi/2)$. Moreover, the second minimum of the $b = d_{dp}$ curve becomes the global minimum unlike that for $(\phi_A, \phi_B) = (\pi/2, \pi/2)$.

In order to understand in detail how the superposition of gluon waves produced by different dipole orientations is responsible for the above (ϕ_A, ϕ_B) -integrated results, we show v_2^x for $(\phi_A, \phi_B) = (0, \pi/2)$ and $(\pm\pi/4, \pi/2)$ in comparison with $(\phi_A, \phi_B) = (\pi/2, \pi/2)$ respectively for $b = 0.5d_{dp}$ (left) and $b = d_{dp}$ (right) in Fig. 3.

As shown in both plots of Fig. 3, at low k_T (with $k_T d_{dp} < 3$) only the $(0, \pi/2)$ curve is positive, which peaks at about the same value of k_T as the first minimum of the corresponding $(\pi/2, \pi/2)$ curve. That is, around this region it is superposed destructively with the $(\pi/2, \pi/2)$ curve in its contribution to the (ϕ_A, ϕ_B) -integrated v_2^x . And this is consistent with the fact that the minimum in the $(\pi/2, \pi/2)$ curve around this region is destroyed and the (ϕ_A, ϕ_B) -integrated v_2^x instead develops its first minimum at lower k_T for both values of

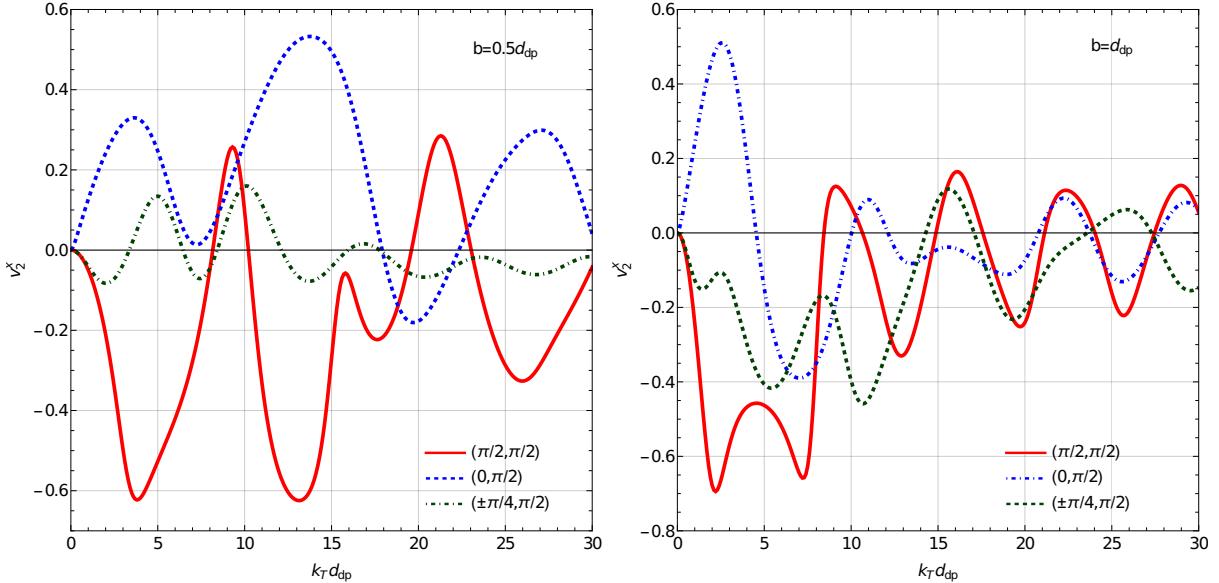


FIG. 3. v_2^x as a function of k_T for different values of (ϕ_A, ϕ_B) at $b = 0.5d_{dp}$ (left) and $b = d_{dp}$ (right).

b as observed in Fig. 2.

At higher k_T the $(\pi/2, \pi/2)$ curve for $b = 0.5d_{dp}$ (in the left plot of Fig. 3) changes its sign and develops a maximum while the one for $b = d_{dp}$ (in the right plot of Fig. 3) never changes its sign before developing another minimum around $k_T = 7.5d_{dp}^{-1}$, as first shown in Fig. 1. All the other curves for $b = d_{dp}$ are negative around the location of the second minimum of the $(\pi/2, \pi/2)$ curve. Accordingly, the gluon waves from these dipole orientations are all superposed constructively in their contributions to the (ϕ_A, ϕ_B) -integrated v_2^x . In contrast, for $b = 0.5d_{dp}$ one can not convincingly identify a higher k_T region dominated by such constructive superposition.

3. The azimuthal distribution for different dipole orientations

At the end, we study the azimuthal distribution defined as a two-dimensional vector: $\frac{1}{\hat{\sigma}} \frac{d\hat{\sigma}}{d\phi} (\cos \phi, \sin \phi)$. For brevity $\hat{\sigma}$ here denotes the ϕ -integrated differential dipole cross section at given η , k_T and b , according to eq. (35). The magnitude of this vector represents the probability density for the gluon to be emitted at an angle ϕ with respect to the x -axis. And in the azimuthal distribution plot the flow angle $\psi_2 = \psi_{\mathbf{v}_2}/2$ can be intuitively estimated as the angle of the long-axis of an ellipse (or a “spindle”) tightly enclosing the distribution

curve.

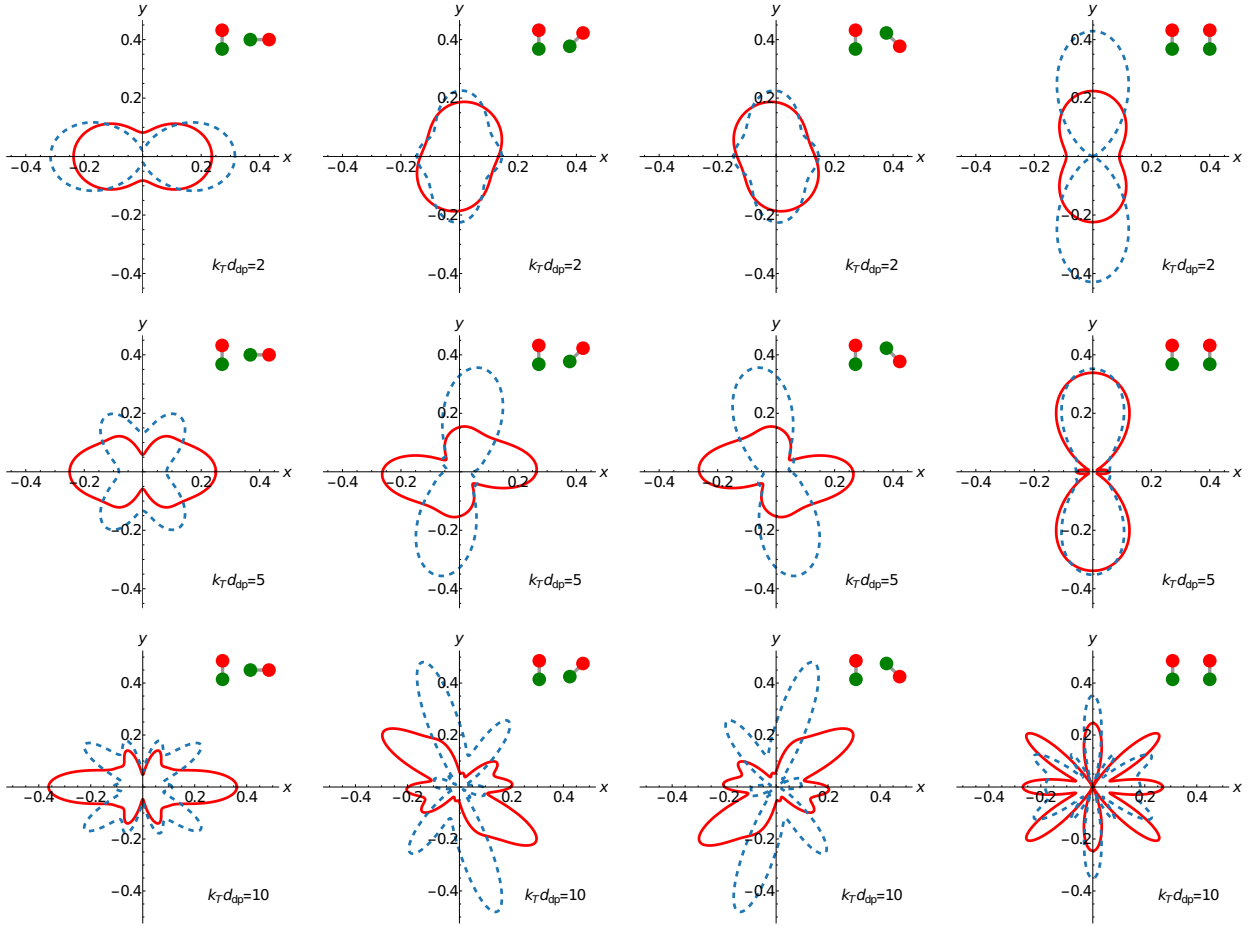


FIG. 4. The azimuthal distribution $\frac{1}{\delta} \frac{d\hat{\sigma}}{d\phi}(\cos \phi, \sin \phi)$ at $b = 0.5d_{dp}$ (red solid) and $b = d_{dp}$ (blue dashed) for $k_T d_{dp} = 2, 5$ and 10 . The dipole orientations are illustrated in the top right corner of the plots.

The azimuthal distributions at $k_T = 2d_{dp}^{-1}$, $5d_{dp}^{-1}$ and $10d_{dp}^{-1}$ for the same dipole orientations as those in Fig. 3 are shown in Fig. 4. At $k_T = 2d_{dp}^{-1}$ (the first row in this figure), the distributions for both $b = 0.5d_{dp}$ (red solid) and $b = d_{dp}$ (blue dashed) are qualitatively very similar for all the shown 4 dipole orientations: Only for $(\phi_A, \phi_B) = (0, \pi/2)$ the gluon is most probably emitted along the x -axis, so $\psi_2 = 0$ and $\phi_{v_2} = 0$, corresponding to a positive v_2^x . For the other 3 dipole orientations the most probable direction to emit a gluon is close to the y -axis, corresponding to a negative v_2^x .

The plots in the second row of Fig. 4 show the azimuthal distributions at $k_T = 5d_{dp}^{-1}$. Only for $(\phi_A, \phi_B) = (\pi/2, \pi/2)$, v_2^x remains negative for both values of b . For $(\phi_A, \phi_B) = (0, \pi/2)$,

it is evident that the most probable emission still occurs along the x -axis for $b = 0.5d_{dp}$ while it is, after eliminating higher harmonics, along the y -axis for $b = d_{dp}$ (that is, its v_2^x becomes negative). For $(\phi_A, \phi_B) = (\pm\pi/4, \pi/2)$, v_2^x at $b = 0.5d_{dp}$ changes its sign and becomes positive while v_2^x at $b = d_{dp}$ remains negative. As a result, the distributions from the 4 dipole orientations are superposed constructively for $b = d_{dp}$ but destructively for $b = 0.5d_{dp}$ when (ϕ_A, ϕ_B) are integrated over.

The azimuthal distributions at $k_T = 10d_{dp}^{-1}$ are shown in the last row of Fig. 4. For both values of b , the distributions become more oscillatory than low k_T (it becomes even more so at higher k_T). The values of v_2^x at $b = 0.5d_{dp}$ are positive for all the four dipole orientations, and v_2^x at $b = d_{dp}$ is negative for $(\phi_A, \phi_B) = (\pm\pi/4, \pi/2)$ and close to 0 for the other two orientations, cf. Fig. 3. Superposing all the highly oscillatory distributions in the (ϕ_A, ϕ_B) space, as illustrated by these dipole orientations, tends to isotropize the gluon emission. This is consistent with the fact that the single-parton distributions (thickness beam functions), used to describe hard processes, are isotropic. Therefore, such a highly oscillatory behavior at high k_T could be viewed as an evidence for the validity of QCD factorization.

V. MOMENTUM ANISOTROPIES IN PION-PION COLLISIONS

In this section we study momentum anisotropies in pion-pion collisions by convoluting the dipole cross section with pion wave functions. Prior to discussing our main results, we first briefly review the LFWFs used in our calculations.

A. The light-front wave function

From a previous work [83], we obtain the LFWF for the low-lying states in the light meson system. Within the valence $|q\bar{q}\rangle$ Fock sector, the state vector of a meson h reads

$$\begin{aligned}
|\psi_h(P, j, m_j)\rangle &= \sum_{s_q, s_{\bar{q}}} \int_0^1 \frac{d\xi}{2\xi(1-\xi)} \int \frac{d^2\mathbf{k}}{(2\pi)^3} \psi_{s_q, s_{\bar{q}}/h}^{(m_j)}(\mathbf{k}, \xi) \\
&\times \frac{1}{\sqrt{N_c}} \sum_{i=1}^{N_c} b_{s_q i}^\dagger(\xi P^+, \mathbf{k} + \xi \mathbf{P}) d_{s_{\bar{q}} i}^\dagger((1-\xi)P^+, -\mathbf{k} + (1-\xi)\mathbf{P})|0\rangle, \quad (69)
\end{aligned}$$

where $P = (P^-, P^+, \mathbf{P})$ is the four momentum of the meson, j and m_j are respectively the total angular momentum and its magnetic projection. Here, $\psi_{s_q s_{\bar{q}}/h}^{(m_j)}(\mathbf{k}, \xi)$ are the valence-sector

LFWFs, where s_q and $s_{\bar{q}}$ represent the spins of the quark and the anti-quark respectively. For simplicity, we write $s = s_q$ and $\bar{s} = s_{\bar{q}}$. Explicitly, we expand the LFWF into the transverse and longitudinal basis functions with coefficients $\psi_h(n, m, l, s, \bar{s})$. In momentum space,

$$\psi_{s\bar{s}/h}(\mathbf{k}, \xi) = \sum_{n,m,l} \psi_h(n, m, l, s, \bar{s}) \phi_{nm}\left(\frac{\mathbf{k}}{\sqrt{\xi(1-\xi)}}\right) \chi_l(\xi), \quad (70)$$

where the basis functions are defined as

$$\begin{aligned} \phi_{nm}(\mathbf{q}) &= \frac{1}{\kappa} \sqrt{\frac{4\pi n!}{(n+|m|)!}} \left(\frac{|\mathbf{q}|}{\kappa}\right)^{|m|} e^{-\frac{|\mathbf{q}|^2}{2\kappa^2}} L_n^{|m|}\left(\frac{|\mathbf{q}|^2}{\kappa^2}\right) e^{im\theta_q}, \\ \chi_l(\xi; \alpha, \beta) &= \xi^{\frac{\beta}{2}} (1-\xi)^{\frac{\alpha}{2}} P_l^{(\alpha, \beta)}(2\xi-1) \sqrt{4\pi(2l+\alpha+\beta+1)} \\ &\quad \times \sqrt{\frac{\Gamma(l+1)\Gamma(l+\alpha+\beta+1)}{\Gamma(l+\alpha+1)\Gamma(l+\beta+1)}}. \end{aligned} \quad (71)$$

Here, in the transverse direction, we use 2D harmonic oscillator basis functions, where $\theta_q = \arg(\mathbf{q})$, and $L_n^a(z)$ is the generalized Laguerre polynomial. Integers n and m are the principal quantum number for radial excitations and the orbital angular momentum projection quantum numbers, respectively. With this, the total angular momentum projection is $m_j = m + s + \bar{s}$. In the longitudinal basis direction, we use modified Jacobi polynomial $P_l^{(\alpha, \beta)}(z)$, where l is the longitudinal quantum number. We have only two free parameters, κ and m_q , from the model Hamiltonian when solving the meson spectroscopy; specifically, we use $\kappa = 610$ MeV and $m_q = 480$ MeV from fitting the ρ meson mass and the pion mass [83]. The confining strength κ also serves as the harmonic oscillator scale parameter. The quantities α and β are dimensionless basis variables, and in the limit of two equal quark masses ($m_q = m_{\bar{q}}$), $\alpha = \beta = 4m_q^2/\kappa^2$.

By Fourier transformation, the LFWF in coordinate space becomes,

$$\tilde{\psi}_{s\bar{s}/h}(\mathbf{r}, \xi) = \sqrt{\xi(1-\xi)} \sum_{n,m,l} \psi_h(n, m, l, s, \bar{s}) \tilde{\phi}_{nm}(\sqrt{\xi(1-\xi)}\mathbf{r}) \chi_l(\xi), \quad (72)$$

where the 2D basis functions in position space are defined as

$$\tilde{\phi}_{nm}(\rho) = \kappa \sqrt{\frac{n!}{\pi(n+|m|)!}} \left(\kappa|\rho|\right)^{|m|} e^{-\frac{\kappa^2|\rho|^2}{2}} L_n^{|m|}(\kappa^2|\rho|^2) e^{im\theta_q + i\pi(n+|m|/2)}. \quad (73)$$

Finally, the LFWFs are respectively normalized according to

$$\sum_{s,\bar{s}} \int_0^1 \frac{d\xi}{2\xi(1-\xi)} \int \frac{d^2\mathbf{k}}{(2\pi)^3} \psi_{s\bar{s}/h'}^{(m'_j)*}(\mathbf{k}, \xi) \psi_{s\bar{s}/h}^{(m_j)}(\mathbf{k}, \xi) = \delta_{hh'} \delta_{m_j m'_j}, \quad (74a)$$

$$\sum_{s,\bar{s}} \int_0^1 \frac{d\xi}{4\pi} \int d^2\mathbf{r} \tilde{\psi}_{s\bar{s}/h'}^{(m'_j)*}(\mathbf{r}, \xi) \tilde{\psi}_{s\bar{s}/h}^{(m_j)}(\mathbf{r}, \xi) = \delta_{hh'} \delta_{m_j m'_j}. \quad (74b)$$

With the basis functions defined, the LFWFs were numerically solved in a truncated basis [83], $N_{\max} = 8$ and $L_{\max} = 24$, giving sufficient energy resolution in both transverse and longitudinal directions: $2n + |m| + 1 \leq N_{\max}$ and $0 \leq l \leq L_{\max}$. In the case of the pion, the leading contributions are summarized in Table I. Although the $(n, m, l) = (0, 0, 0)$, $(0, 1, 0)$, and $(1, 0, 0)$ components contribute the most in the wave function, other higher order quantum numbers (400 in total) also play a significant role in shaping the complete wave function and in determining various observables.

Since spin sums of the squared LFWFs directly enter in the cross section calculations, as in eq. (23), we define a convenient short-hand variable

$$U(\mathbf{r}, \xi) = \sum_{s\bar{s}} |\tilde{\psi}_{s\bar{s}}(\mathbf{r}, \xi)|^2 = |\tilde{\psi}_{\uparrow\downarrow}(\mathbf{r}, \xi)|^2 + |\tilde{\psi}_{\downarrow\uparrow}(\mathbf{r}, \xi)|^2 + |\tilde{\psi}_{\downarrow\downarrow}(\mathbf{r}, \xi)|^2 + |\tilde{\psi}_{\uparrow\uparrow}(\mathbf{r}, \xi)|^2, \quad (75)$$

where $U(\mathbf{r}, \xi) = U(|\mathbf{r}|, \xi)$ is azimuthally symmetric and normalized by $\int_0^1 \frac{d\xi}{4\pi} \int d^2\mathbf{r} U(\mathbf{r}, \xi) = 1$.

In terms of the full and leading quantum numbers,

$$U_{\text{full}}(r, \xi) = \left| \sum_{nml} \tilde{\psi}_{nml\uparrow\downarrow}(r, \xi) \right|^2 + \left| \sum_{nml} \tilde{\psi}_{nml\downarrow\uparrow}(r, \xi) \right|^2 + \left| \sum_{nml} \tilde{\psi}_{nml\downarrow\downarrow}(r, \xi) \right|^2 + \left| \sum_{nml} \tilde{\psi}_{nml\uparrow\uparrow}(r, \xi) \right|^2, \quad (76a)$$

$$U_{000}(r, \xi) = \left| \frac{1}{\sqrt{2}} \tilde{\psi}_{000\uparrow\downarrow}(r, \xi) \right|^2 + \left| \frac{-1}{\sqrt{2}} \tilde{\psi}_{000\downarrow\uparrow}(r, \xi) \right|^2 = |\tilde{\psi}_{000}(r, \xi)|^2, \quad (76b)$$

$$U_{010}(r, \xi) = |\tilde{\psi}_{010\downarrow\downarrow}(r, \xi)|^2 = U_{0-10} = |\tilde{\psi}_{0-10\uparrow\uparrow}(r, \xi)|^2. \quad (76c)$$

Selected density plots of $U(r, \xi)$ are included in Fig. 5. Figures 5(a), 5(b) and 5(c) show $U_{000}(r, \xi)$, $U_{010}(r, \xi)$, and the full LFWF squared, $U_{\text{full}}(r, \xi)$, by summing contributions from all 400 basis functions. To study the sensitivity of physical observables on the number of basis states, we use the notation $U_{\text{top } x \times 4}$ to describe the leading spin-summed squared LFWFs with the first x dominant components in each of the four spin configurations. For example, $U_{\text{top } 100 \times 4} \equiv U_{\text{full}}$ while $U_{\text{top } 5 \times 4}$ has about 95% of the LFWF, which means the

TABLE I. Leading basis functions for pions, ordered by LFWF coefficients $\psi_h(n, m, l, s, \bar{s})$. Recall that $m_j = m + s + \bar{s}$ by momentum conservation, and s, \bar{s} are half integers. We can construct LFWFs using eq. (72) and eq. (70).

n	m	l	s	\bar{s}	$\psi_h(n, m, l, s, \bar{s})$
0	0	0	-1/2	1/2	-0.442466
0	0	0	1/2	-1/2	0.442466
0	1	0	-1/2	-1/2	-0.29865
0	-1	0	1/2	1/2	-0.29865
1	0	0	-1/2	1/2	0.234734
1	0	0	1/2	-1/2	-0.234734

probability of finding the pion in the top 5×4 basis states is about 95%, assuming that the pion is 100% in the full LFWF. Comparing U_{full} and $U_{\text{top } 5 \times 4}$, as shown in Fig. 5(c) and Fig. 5(d), one can see the important contribution of higher-order basis states. In terms of physical observables, the root-mean-square charge radius (r.m.s. radius) is defined as the slope of the charge form factor $F_{ch}(Q^2)$ (FF) at zero momentum transfer,

$$\langle r_c^2 \rangle = -6 \frac{\partial}{\partial Q^2} F_{ch}(Q^2)|_{Q \rightarrow 0}, \quad (77)$$

which can also be equivalently and conveniently obtained by the Burkardt's impact parameter $\mathbf{b} = (1-x)\mathbf{r}$ [79] via

$$\begin{aligned} \langle r_c^2 \rangle &= \frac{3}{2} \langle \mathbf{b}^2 \rangle = \frac{3}{2} \sum_{s, \bar{s}} \int_0^1 \frac{d\xi}{4\pi} \int d^2\mathbf{r} (1-\xi)^2 \mathbf{r}^2 \tilde{\psi}_{s\bar{s}/h'}^*(\mathbf{r}, \xi) \tilde{\psi}_{s\bar{s}/h}(\mathbf{r}, \xi) \\ &= \frac{3}{2} \int_0^1 \frac{d\xi}{4\pi} \int d^2\mathbf{r} (1-\xi)^2 \mathbf{r}^2 U(\mathbf{r}, \xi), \end{aligned} \quad (78)$$

where we summarize calculations of the r.m.s. radius of the pion in Table II.

B. Transverse momentum anisotropies

By plugging the dipole cross section evaluated in sec. III C and the pion wave functions in the previous subsection into eq. (23), we now study transverse momentum anisotropies⁶

⁶ The LO formula in eq. (35) produces non-vanishing even flow coefficients for $b > 0$. We find that, e.g., v_4 , with v_4^x of opposite sign than v_2^x , is about one order of magnitude smaller than v_2 at the same b . In this section we only focus on the dominant flow coefficient v_2 .

TABLE II. The pion r.m.s. charge radius $\sqrt{\langle r_c^2 \rangle}$ (in fm) calculated using eq. (78) for various components of LFWFs, partial LFWFs and the full LFWFs. The charge radii are also plotted in Fig. 5 respectively. For comparison, the PDG data for the charge radius is 0.659 fm [103].

	(0, 0, 0)	(0, ± 1 , 0)	$U_{\text{top } 5 \times 4}$	U_{full}
$\sqrt{\langle r_c^2 \rangle}$	0.469	0.664	0.40	0.44

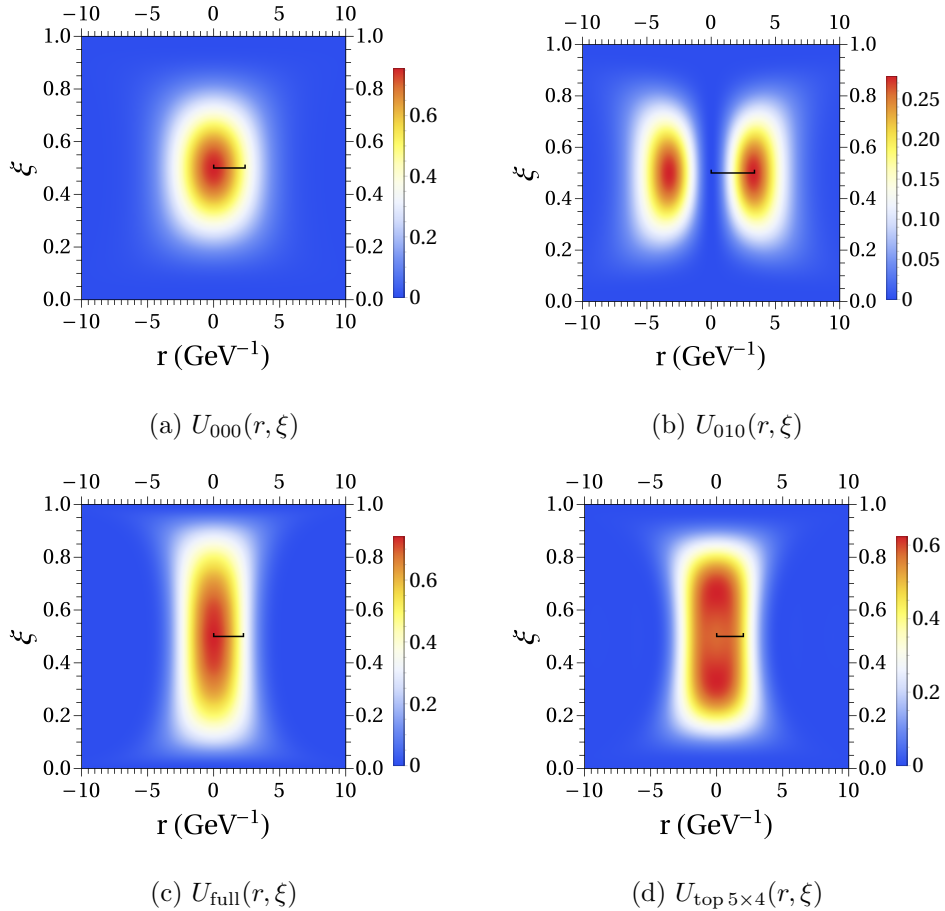


FIG. 5. Selected density plots of squared pion LFWFs according to eq. (75). The black segment shown on each plot represents the respective pion r.m.s. radius calculated using eq. (78).

in high-energy pion-pion collisions. The results presented below are all obtained by using Monte Carlo methods [104, 105] to carry out the integration over \mathbf{r}_i , ξ_i and ϕ numerically.

For our choice of the coordinates in eq. (51) in which the reaction plane coincides with the x - z plane, one has $v_2^y = 0$ due to reflection symmetry over the x -axis in the pion wave function squared (see eq. (55) for the definition of $\mathbf{v}_n = (v_n^x, v_n^y)$). And we find that

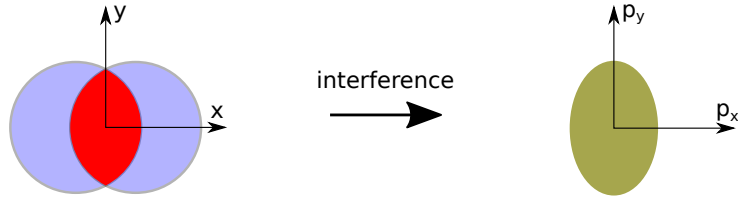


FIG. 6. Collision geometry and transverse momentum anisotropies. According to our choice of the coordinates in eq. (51), the reaction plane in the corresponding classical picture coincides with the x - z plane. And the gluon is found to be more probably produced along the y -axis than the x -axis due to interference.

v_2^x shown below is negative and, equivalently, the flow angle $\psi_2 = \pi/2$, as illustrated in Fig. 6. It is qualitatively different from the expectation by naively extrapolating the classical hydrodynamic interpretation of elliptic flow in heavy-ion collisions [106] to hadron-hadron collisions. It would instead predict $\psi_2 = 0$, the same as the reaction plane angle. It is also different from the one-hit result in kinetic theory, which also has $\psi_2 = 0$ (see, e.g., ref. [33]).

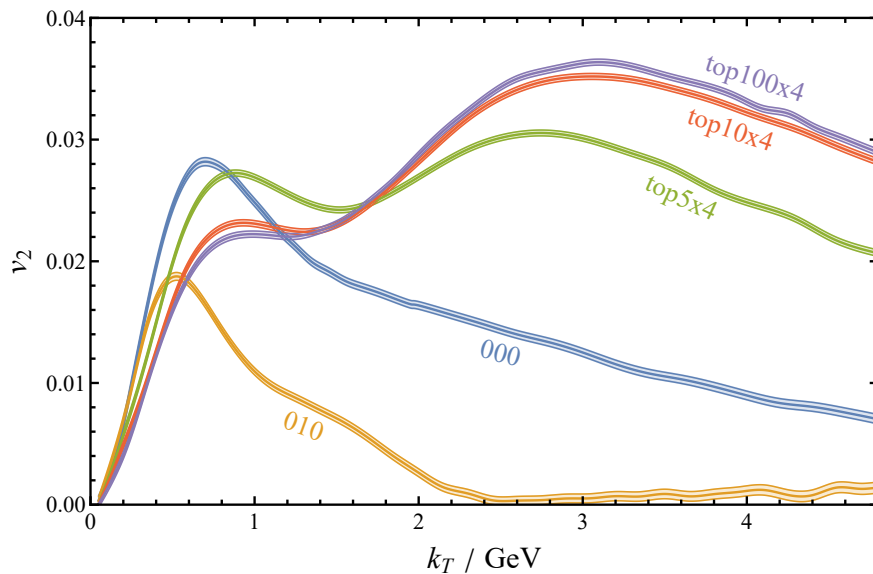


FIG. 7. Sensitivity of v_2 on the shape of the pion light-front wave functions. The plot shows the results of v_2 for U_{000} , U_{010} , $U_{\text{top}5 \times 4}$, $U_{\text{top}10 \times 4}$ and $U_{\text{top}100 \times 4}$ (i.e., the full LFWF squared) at $b = 0.2$ fm; see definitions of U s in eq. (76) and associated discussions. Here, the error bands are estimated as the uncertainties in Monte Carlo integration.

Fig. 7 shows the results of $v_2 = |v_2^x|$ at $b = 0.2$ fm by using one (U_{000} and U_{010}), top 5

($U_{\text{top } 5 \times 4}$), top 10 ($U_{\text{top } 10 \times 4}$) and top 100 ($U_{\text{full}} = U_{\text{top } 100 \times 4}$) spin-summed, squared LFWFs. From this figure one can see that the shape of v_2 is quite sensitive to that of the wave functions, cf. Fig. 5. Even $U_{\text{top } 5 \times 4}$ produces a noticeably different shape of v_2 than the full one. Only if enough basis functions (top 10×4 or more) are included, v_2 stabilizes (note the probability for the pion to occupy the basis states in U_{full} not contained in $U_{\text{top } 10 \times 4}$ is only about 1%). For a comparison, the values of the r.m.s. charge radius for U_{000} , U_{010} , $U_{\text{top } 5 \times 4}$ and U_{full} are listed in Table II, which do not show such a strong dependence on the shape of the wave functions (except U_{010}). Therefore, transverse momentum anisotropies could be used as a unique, stringent constraint on the shape of the hadron wave function, especially its high excited basis states.

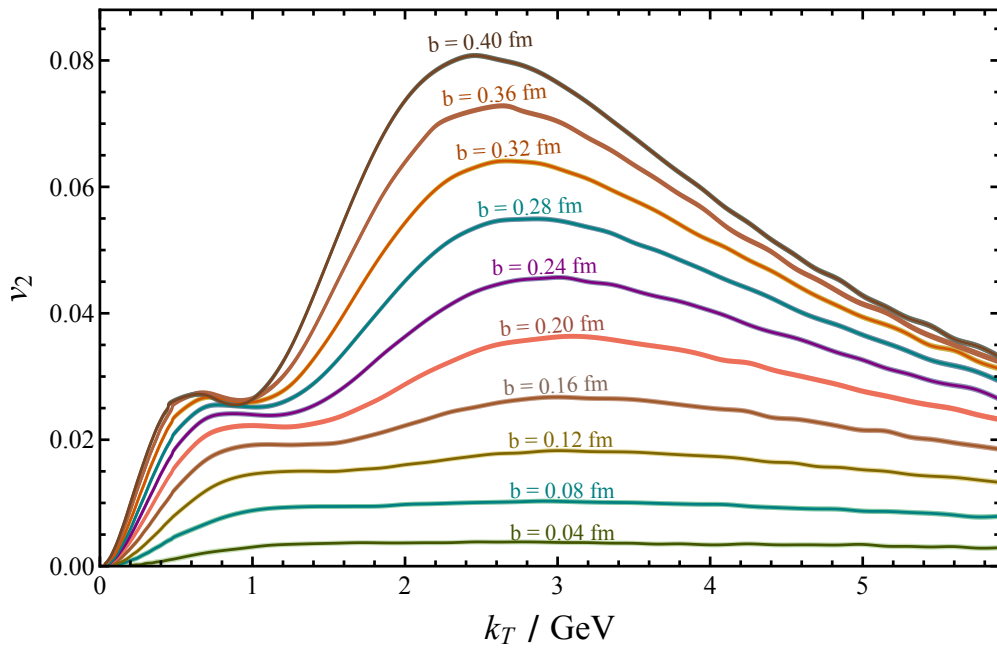


FIG. 8. The elliptic flow v_2 as a function of k_T at different impact parameters in pion-pion collisions. The collision geometry in the classical picture corresponding to each value of b could be inferred from the pion r.m.s. charge radius $\sqrt{\langle r_c^2 \rangle} = 0.44$ fm.

The pion v_2 at different impact parameters, calculated with the full LFWF, is shown as a function of k_T in Fig. 8. From central ($b = 0.04$ fm) to peripheral ($b = 0.4$ fm) collisions, v_2 always increases in the full range of $k_T \leq 6$ GeV (except for the curve with $b = 0.4$ fm at $0.6 \text{ GeV} \lesssim k_T \lesssim 1 \text{ GeV}$). At low k_T the quadratic growth survives in pion-pion collisions although the range of such a low- k_T behavior is normally shortened compared to that in

dipole-dipole collisions, as shown in Fig. 2. The qualitative behavior of v_2 for larger k_T depends on the centrality of the collision. For $b > 0.1$ fm, v_2 is characterized by a double-peak structure in which the global maximum locates in the range of $k_T = 2 - 4$ GeV. Such a distinct structure becomes more pronounced at larger b . This qualitatively agrees with our observation in dipole-dipole scattering, cf. Fig. 2.

The double-peak structure in v_2 is a characteristic feature of the interference effect as discussed in sec. IV. Let us take for example $b \sim \sqrt{\langle r_c^2 \rangle}$, the pion r.m.s charge radius. In this case, $\sqrt{\langle r_c^2 \rangle} = 0.44$ fm is the only length scale in the problem. We find that the high k_T behavior of v_2 in eq. (68), although failing to predict the magnitude of v_2 for the shown range of k_T , gives a reasonable estimate of the locations of the two minima shown in Fig. 8: the first minimum locates around $k_T \sim 0.25\pi/\sqrt{\langle r_c^2 \rangle} = 0.36$ GeV while the second, around $k_T \sim 2.25\pi/\sqrt{\langle r_c^2 \rangle} = 3.2$ GeV. In addition, both peak locations mitigate to larger k_T for decreasing b , as what one would expect from such an estimation, $k_{T,peak} \approx (0.25, 2.25)\pi/b$. That is, the peak locations are roughly determined by the hadron size (and the impact parameter).

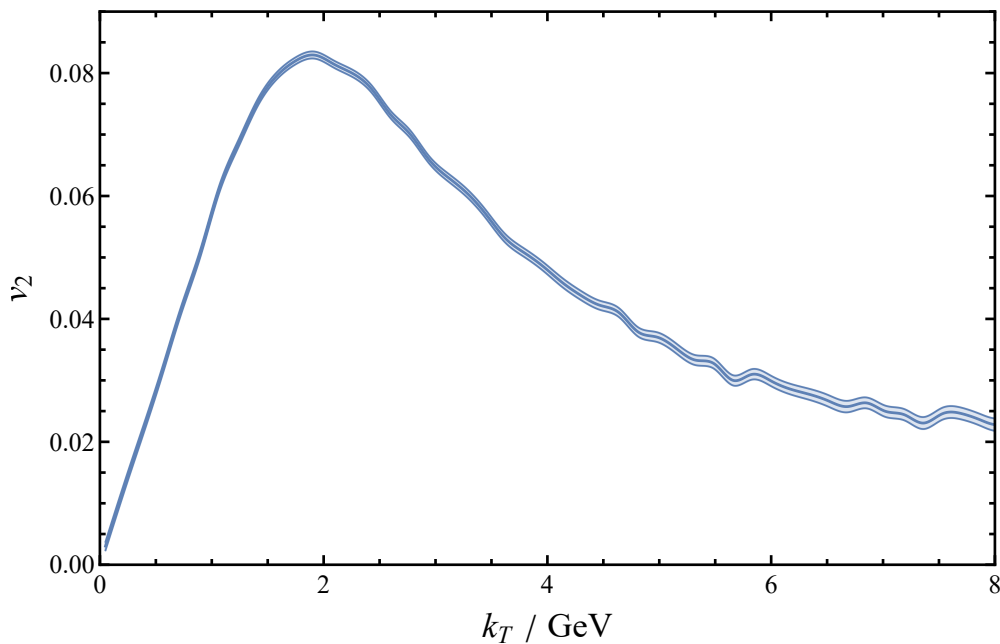


FIG. 9. v_2 as a function of k_T with b integrated in pion-pion collisions.

This paper is not aimed at a detailed discussion of flow phenomenology but to assess quantitatively the relative importance of the contributions to transverse momentum anisotropies from scattering of hadron valence quark skeletons in comparison with other

initial-state and final-state effects [24, 25]. As shown in Fig. 8, with the only two parameters in the LFWFs fixed by light meson masses we find that the predicted v_2 at b about the value of pion r.m.s. charge radius in soft gluon production is comparable to that observed in pp collisions [10, 14, 15, 17, 18, 20, 22, 23] as well as theoretical results [25, 27, 28, 43, 47, 49, 51, 55, 57, 98–100]. Note unlike heavy-ion collisions the impact parameter b would not be well determined in pp collisions at the LHC [92], and we will need to find out its correlation with measurable quantities such as multiplicity in detailed phenomenological studies. In order to exemplify the effects of averaging over the impact parameter, we show the result of v_2 with b integrated in Fig. 9. The maximum of the b -integrated v_2 (≈ 0.08), similar to that with $b \approx \sqrt{\langle r_c^2 \rangle}$, is found to develop at lower $k_T \approx 2$ GeV while the double-peak structure is averaged out. The absence of the left peak is a combined effect of the large cross section with small b and the large anisotropy with large b . Based on our observations in Figs. 8 and 9, we believe that the interference effect from the emitters of valence (anti)quarks as discussed above would not be negligible in a comprehensive study of flow phenomenology. For example, if the events with large b could be isolated, one could in principle observe the double-peak structure.

There are many issues to be addressed before we attempt to carry out phenomenological studies of collectivity in hadron-hadron collisions. First, since the proton wave functions are already available [88–91], it would be intriguing and experimentally more relevant to generalize our calculations to proton-proton collisions. Second, in parton saturation/small- x physics it was found that the contributions of the small- x evolution could be significant in the description of collectivity [45, 46]. It, hence, would be of significance to study the effects of the small- x evolution [94–97] on our LO results as well. Third, collectivity in multiple gluon production (higher-order cumulants) has been studied with [67] or without [70, 71] saturated dense gluons and transverse momentum anisotropies were found to persist. It would be important for us to carry out high-order calculations to study multi-particle correlations to confirm that observation. Fourth, either hadronization, the Local Parton-Hadron Duality [107] or some physical observable such as the transverse energy needs to be introduced in order to compare with experimental data. Last but not least, the general formula for the impact-parameter dependent cross section in eq. (1) is valid beyond the eikonal limit, which allows the exploration of non-eikonal effects. Such effects were shown to be sizable, e.g., at RHIC energies in CGC [65, 66, 68, 69]. All these questions are left for

future research.

ACKNOWLEDGMENTS

We thank Nestor Armesto, Zhenyu Chen, Yuri Kovchegov, James P. Vary, Carlos Salgado, Yu Shi, Bo-Wen Xiao, and Xingbo Zhao for insightful discussions. This work is supported by European Research Council project ERC-2018-ADG-835105 YoctoLHC; by Maria de Maetzu excellence program under project CEX2020-001035-M; by Spanish Research State Agency under project PID2020-119632GB-I00; and by Xunta de Galicia (Centro singular de investigación de Galicia accreditation 2019-2022), by European Union ERDF. H.Z. is supported by the National Natural Science Foundation of China (NSFC) under Grant No. 12075136. B.W. acknowledges the support of the Ramón y Cajal program with the Grant No. RYC2021-032271-I.

-
- [1] U. Heinz and R. Snellings, *Collective flow and viscosity in relativistic heavy-ion collisions*, *Ann. Rev. Nucl. Part. Sci.* **63** (2013) 123 [[1301.2826](#)].
 - [2] CMS collaboration, *Observation of Long-Range Near-Side Angular Correlations in Proton-Proton Collisions at the LHC*, *JHEP* **09** (2010) 091 [[1009.4122](#)].
 - [3] CMS collaboration, *Observation of Long-Range Near-Side Angular Correlations in Proton-Lead Collisions at the LHC*, *Phys. Lett. B* **718** (2013) 795 [[1210.5482](#)].
 - [4] ALICE collaboration, *Long-range angular correlations on the near and away side in p-Pb collisions at $\sqrt{s_{NN}} = 5.02$ TeV*, *Phys. Lett. B* **719** (2013) 29 [[1212.2001](#)].
 - [5] ATLAS collaboration, *Observation of Associated Near-Side and Away-Side Long-Range Correlations in $\sqrt{s_{NN}}=5.02$ TeV Proton-Lead Collisions with the ATLAS Detector*, *Phys. Rev. Lett.* **110** (2013) 182302 [[1212.5198](#)].
 - [6] CMS collaboration, *Multiplicity and Transverse Momentum Dependence of Two- and Four-Particle Correlations in pPb and PbPb Collisions*, *Phys. Lett. B* **724** (2013) 213 [[1305.0609](#)].
 - [7] ALICE collaboration, *Multiparticle azimuthal correlations in p-Pb and Pb-Pb collisions at the CERN Large Hadron Collider*, *Phys. Rev. C* **90** (2014) 054901 [[1406.2474](#)].

- [8] CMS collaboration, *Long-range two-particle correlations of strange hadrons with charged particles in pPb and PbPb collisions at LHC energies*, *Phys. Lett. B* **742** (2015) 200 [[1409.3392](#)].
- [9] CMS collaboration, *Evidence for Collective Multiparticle Correlations in p-Pb Collisions*, *Phys. Rev. Lett.* **115** (2015) 012301 [[1502.05382](#)].
- [10] ATLAS collaboration, *Observation of Long-Range Elliptic Azimuthal Anisotropies in $\sqrt{s} = 13$ and 2.76 TeV pp Collisions with the ATLAS Detector*, *Phys. Rev. Lett.* **116** (2016) 172301 [[1509.04776](#)].
- [11] CMS collaboration, *Measurement of long-range near-side two-particle angular correlations in pp collisions at $\sqrt{s} = 13$ TeV*, *Phys. Rev. Lett.* **116** (2016) 172302 [[1510.03068](#)].
- [12] LHCb collaboration, *Measurements of long-range near-side angular correlations in $\sqrt{s_{NN}} = 5$ TeV proton-lead collisions in the forward region*, *Phys. Lett. B* **762** (2016) 473 [[1512.00439](#)].
- [13] CMS collaboration, *Pseudorapidity dependence of long-range two-particle correlations in pPb collisions at $\sqrt{s_{NN}} = 5.02$ TeV*, *Phys. Rev. C* **96** (2017) 014915 [[1604.05347](#)].
- [14] CMS collaboration, *Evidence for collectivity in pp collisions at the LHC*, *Phys. Lett. B* **765** (2017) 193 [[1606.06198](#)].
- [15] ATLAS collaboration, *Measurement of multi-particle azimuthal correlations in pp, p+Pb and low-multiplicity Pb+Pb collisions with the ATLAS detector*, *Eur. Phys. J. C* **77** (2017) 428 [[1705.04176](#)].
- [16] CMS collaboration, *Pseudorapidity and transverse momentum dependence of flow harmonics in pPb and PbPb collisions*, *Phys. Rev. C* **98** (2018) 044902 [[1710.07864](#)].
- [17] ATLAS collaboration, *Measurement of long-range multiparticle azimuthal correlations with the subevent cumulant method in pp and p + Pb collisions with the ATLAS detector at the CERN Large Hadron Collider*, *Phys. Rev. C* **97** (2018) 024904 [[1708.03559](#)].
- [18] CMS collaboration, *Observation of Correlated Azimuthal Anisotropy Fourier Harmonics in pp and p + Pb Collisions at the LHC*, *Phys. Rev. Lett.* **120** (2018) 092301 [[1709.09189](#)].
- [19] PHENIX collaboration, *Creation of quark-gluon plasma droplets with three distinct geometries*, *Nature Phys.* **15** (2019) 214 [[1805.02973](#)].
- [20] ATLAS collaboration, *Correlated long-range mixed-harmonic fluctuations measured in pp, p+Pb and low-multiplicity Pb+Pb collisions with the ATLAS detector*, *Phys. Lett. B* **789**

- (2019) 444 [[1807.02012](#)].
- [21] CMS collaboration, *Bose-Einstein correlations of charged hadrons in proton-proton collisions at $\sqrt{s} = 13$ TeV*, *JHEP* **03** (2020) 014 [[1910.08815](#)].
- [22] ATLAS collaboration, *Measurement of long-range two-particle azimuthal correlations in Z-boson tagged pp collisions at $\sqrt{s}=8$ and 13 TeV*, *Eur. Phys. J. C* **80** (2020) 64 [[1906.08290](#)].
- [23] CMS collaboration, *Studies of charm and beauty hadron long-range correlations in pp and pPb collisions at LHC energies*, *Phys. Lett. B* **813** (2021) 136036 [[2009.07065](#)].
- [24] J.L. Nagle and W.A. Zajc, *Small System Collectivity in Relativistic Hadronic and Nuclear Collisions*, *Ann. Rev. Nucl. Part. Sci.* **68** (2018) 211 [[1801.03477](#)].
- [25] T. Altinoluk and N. Armesto, *Particle correlations from the initial state*, *Eur. Phys. J. A* **56** (2020) 215 [[2004.08185](#)].
- [26] Z. Citron et al., *Report from Working Group 5: Future physics opportunities for high-density QCD at the LHC with heavy-ion and proton beams*, *CERN Yellow Rep. Monogr.* **7** (2019) 1159 [[1812.06772](#)].
- [27] D. d’Enterria, G.K. Eyyubova, V.L. Korotkikh, I.P. Lokhtin, S.V. Petrushanko, L.I. Sarycheva et al., *Estimates of hadron azimuthal anisotropy from multiparton interactions in proton-proton collisions at $\sqrt{s} = 14$ TeV*, *Eur. Phys. J. C* **66** (2010) 173 [[0910.3029](#)].
- [28] P. Bozek, *Elliptic flow in proton-proton collisions at $\sqrt{s} = 7$ TeV*, *Eur. Phys. J. C* **71** (2011) 1530 [[1010.0405](#)].
- [29] P. Bozek, *Collective flow in p-Pb and d-Pd collisions at TeV energies*, *Phys. Rev. C* **85** (2012) 014911 [[1112.0915](#)].
- [30] P. Romatschke and U. Romatschke, *Relativistic Fluid Dynamics In and Out of Equilibrium*, Cambridge Monographs on Mathematical Physics, Cambridge University Press (5, 2019), [10.1017/9781108651998](#), [[1712.05815](#)].
- [31] N. Borghini and C. Gombeaud, *Anisotropic flow far from equilibrium*, *Eur. Phys. J. C* **71** (2011) 1612 [[1012.0899](#)].
- [32] P. Romatschke, *Azimuthal Anisotropies at High Momentum from Purely Non-Hydrodynamic Transport*, *Eur. Phys. J. C* **78** (2018) 636 [[1802.06804](#)].

- [33] A. Kurkela, U.A. Wiedemann and B. Wu, *Nearly isentropic flow at sizeable η/s* , *Phys. Lett. B* **783** (2018) 274 [[1803.02072](#)].
- [34] A. Kurkela, U.A. Wiedemann and B. Wu, *Opacity dependence of elliptic flow in kinetic theory*, *Eur. Phys. J. C* **79** (2019) 759 [[1805.04081](#)].
- [35] A. Kurkela, A. Mazeliauskas and R. Törnkvist, *Collective flow in single-hit QCD kinetic theory*, *JHEP* **11** (2021) 216 [[2104.08179](#)].
- [36] A. Ortiz Velasquez, P. Christiansen, E. Cuautle Flores, I. Maldonado Cervantes and G. Paic, *Color Reconnection and Flowlike Patterns in pp Collisions*, *Phys. Rev. Lett.* **111** (2013) 042001 [[1303.6326](#)].
- [37] M. Greif, C. Greiner, B. Schenke, S. Schlichting and Z. Xu, *Importance of initial and final state effects for azimuthal correlations in p+Pb collisions*, *Phys. Rev. D* **96** (2017) 091504 [[1708.02076](#)].
- [38] A. Kurkela, U.A. Wiedemann and B. Wu, *Flow in AA and pA as an interplay of fluid-like and non-fluid like excitations*, *Eur. Phys. J. C* **79** (2019) 965 [[1905.05139](#)].
- [39] A. Kurkela, S.F. Taghavi, U.A. Wiedemann and B. Wu, *Hydrodynamization in systems with detailed transverse profiles*, *Phys. Lett. B* **811** (2020) 135901 [[2007.06851](#)].
- [40] Z.-W. Lin and L. Zheng, *Further developments of a multi-phase transport model for relativistic nuclear collisions*, *Nucl. Sci. Tech.* **32** (2021) 113 [[2110.02989](#)].
- [41] V.E. Ambrus, S. Schlichting and C. Werthmann, *Establishing the range of applicability of hydrodynamics in high-energy collisions*, [2211.14356](#).
- [42] N. Armesto, L. McLerran and C. Pajares, *Long Range Forward-Backward Correlations and the Color Glass Condensate*, *Nucl. Phys. A* **781** (2007) 201 [[hep-ph/0607345](#)].
- [43] A. Dumitru, K. Dusling, F. Gelis, J. Jalilian-Marian, T. Lappi and R. Venugopalan, *The Ridge in proton-proton collisions at the LHC*, *Phys. Lett. B* **697** (2011) 21 [[1009.5295](#)].
- [44] A. Kovner and M. Lublinsky, *Angular Correlations in Gluon Production at High Energy*, *Phys. Rev. D* **83** (2011) 034017 [[1012.3398](#)].
- [45] E. Levin and A.H. Rezaeian, *The Ridge from the BFKL evolution and beyond*, *Phys. Rev. D* **84** (2011) 034031 [[1105.3275](#)].
- [46] A. Kovner and M. Lublinsky, *On Angular Correlations and High Energy Evolution*, *Phys. Rev. D* **84** (2011) 094011 [[1109.0347](#)].

- [47] K. Dusling and R. Venugopalan, *Azimuthal collimation of long range rapidity correlations by strong color fields in high multiplicity hadron-hadron collisions*, *Phys. Rev. Lett.* **108** (2012) 262001 [[1201.2658](#)].
- [48] Y.V. Kovchegov and D.E. Wertepny, *Long-Range Rapidity Correlations in Heavy-Light Ion Collisions*, *Nucl. Phys. A* **906** (2013) 50 [[1212.1195](#)].
- [49] K. Dusling and R. Venugopalan, *Comparison of the color glass condensate to dihadron correlations in proton-proton and proton-nucleus collisions*, *Phys. Rev. D* **87** (2013) 094034 [[1302.7018](#)].
- [50] Y.V. Kovchegov and D.E. Wertepny, *Two-Gluon Correlations in Heavy-Light Ion Collisions: Energy and Geometry Dependence, IR Divergences, and k_T -Factorization*, *Nucl. Phys. A* **925** (2014) 254 [[1310.6701](#)].
- [51] B. Schenke and R. Venugopalan, *Eccentric protons? Sensitivity of flow to system size and shape in $p+p$, $p+Pb$ and $Pb+Pb$ collisions*, *Phys. Rev. Lett.* **113** (2014) 102301 [[1405.3605](#)].
- [52] A. Dumitru, L. McLerran and V. Skokov, *Azimuthal asymmetries and the emergence of “collectivity” from multi-particle correlations in high-energy pA collisions*, *Phys. Lett. B* **743** (2015) 134 [[1410.4844](#)].
- [53] T. Altinoluk, N. Armesto, G. Beuf, A. Kovner and M. Lublinsky, *Bose enhancement and the ridge*, *Phys. Lett. B* **751** (2015) 448 [[1503.07126](#)].
- [54] T. Lappi, B. Schenke, S. Schlichting and R. Venugopalan, *Tracing the origin of azimuthal gluon correlations in the color glass condensate*, *JHEP* **01** (2016) 061 [[1509.03499](#)].
- [55] B. Schenke, S. Schlichting, P. Tribedy and R. Venugopalan, *Mass ordering of spectra from fragmentation of saturated gluon states in high multiplicity proton-proton collisions*, *Phys. Rev. Lett.* **117** (2016) 162301 [[1607.02496](#)].
- [56] A. Kovner, M. Lublinsky and V. Skokov, *Exploring correlations in the CGC wave function: odd azimuthal anisotropy*, *Phys. Rev. D* **96** (2017) 016010 [[1612.07790](#)].
- [57] E. Iancu and A.H. Rezaeian, *Elliptic flow from color-dipole orientation in pp and pA collisions*, *Phys. Rev. D* **95** (2017) 094003 [[1702.03943](#)].
- [58] K. Dusling, M. Mace and R. Venugopalan, *Multiparticle collectivity from initial state correlations in high energy proton-nucleus collisions*, *Phys. Rev. Lett.* **120** (2018) 042002 [[1705.00745](#)].

- [59] K. Dusling, M. Mace and R. Venugopalan, *Parton model description of multiparticle azimuthal correlations in pA collisions*, *Phys. Rev. D* **97** (2018) 016014 [[1706.06260](#)].
- [60] Y.V. Kovchegov and V.V. Skokov, *How classical gluon fields generate odd azimuthal harmonics for the two-gluon correlation function in high-energy collisions*, *Phys. Rev. D* **97** (2018) 094021 [[1802.08166](#)].
- [61] M. Mace, V.V. Skokov, P. Tribedy and R. Venugopalan, *Hierarchy of Azimuthal Anisotropy Harmonics in Collisions of Small Systems from the Color Glass Condensate*, *Phys. Rev. Lett.* **121** (2018) 052301 [[1805.09342](#)].
- [62] T. Altinoluk, N. Armesto, A. Kovner and M. Lublinsky, *Double and triple inclusive gluon production at mid rapidity: quantum interference in p-A scattering*, *Eur. Phys. J. C* **78** (2018) 702 [[1805.07739](#)].
- [63] M. Mace, V.V. Skokov, P. Tribedy and R. Venugopalan, *Systematics of azimuthal anisotropy harmonics in proton–nucleus collisions at the LHC from the Color Glass Condensate*, *Phys. Lett. B* **788** (2019) 161 [[1807.00825](#)].
- [64] M.K. Davy, C. Marquet, Y. Shi, B.-W. Xiao and C. Zhang, *Two particle azimuthal harmonics in pA collisions*, *Nucl. Phys. A* **983** (2019) 293 [[1808.09851](#)].
- [65] P. Agostini, T. Altinoluk and N. Armesto, *Effect of non-eikonal corrections on azimuthal asymmetries in the Color Glass Condensate*, *Eur. Phys. J. C* **79** (2019) 790 [[1907.03668](#)].
- [66] P. Agostini, T. Altinoluk and N. Armesto, *Non-eikonal corrections to multi-particle production in the Color Glass Condensate*, *Eur. Phys. J. C* **79** (2019) 600 [[1902.04483](#)].
- [67] P. Agostini, T. Altinoluk and N. Armesto, *Multi-particle production in proton–nucleus collisions in the color glass condensate*, *Eur. Phys. J. C* **81** (2021) 760 [[2103.08485](#)].
- [68] P. Agostini, T. Altinoluk, N. Armesto, F. Dominguez and J.G. Milhano, *Multiparticle production in proton–nucleus collisions beyond eikonal accuracy*, *Eur. Phys. J. C* **82** (2022) 1001 [[2207.10472](#)].
- [69] P. Agostini, T. Altinoluk and N. Armesto, *Finite width effects on the azimuthal asymmetry in proton-nucleus collisions in the Color Glass Condensate*, [2212.03633](#).
- [70] B. Blok, C.D. Jäkel, M. Strikman and U.A. Wiedemann, *Collectivity from interference*, *JHEP* **12** (2017) 074 [[1708.08241](#)].
- [71] B. Blok and U.A. Wiedemann, *Collectivity in pp from resummed interference effects?*, *Phys. Lett. B* **795** (2019) 259 [[1812.04113](#)].

- [72] A. Dumitriu and R. Paatelainen, *Sub-femtometer scale color charge fluctuations in a proton made of three quarks and a gluon*, *Phys. Rev. D* **103** (2021) 034026 [[2010.11245](#)].
- [73] S.J. Brodsky, H.-C. Pauli and S.S. Pinsky, *Quantum chromodynamics and other field theories on the light cone*, *Phys. Rept.* **301** (1998) 299 [[hep-ph/9705477](#)].
- [74] J.P. Vary, H. Honkanen, J. Li, P. Maris, S.J. Brodsky, A. Harindranath et al., *Hamiltonian light-front field theory in a basis function approach*, *Phys. Rev. C* **81** (2010) 035205 [[0905.1411](#)].
- [75] G.F. de Teramond and S.J. Brodsky, *Light-Front Holography: A First Approximation to QCD*, *Phys. Rev. Lett.* **102** (2009) 081601 [[0809.4899](#)].
- [76] S.J. Brodsky, G.F. de Teramond, H.G. Dosch and J. Erlich, *Light-Front Holographic QCD and Emerging Confinement*, *Phys. Rept.* **584** (2015) 1 [[1407.8131](#)].
- [77] S.J. Brodsky, G.F. de Teramond and H.G. Dosch, *Light-Front Holography and Supersymmetric Conformal Algebra: A Novel Approach to Hadron Spectroscopy, Structure, and Dynamics*, 4, 2020 [[2004.07756](#)].
- [78] Y. Li, P. Maris, X. Zhao and J.P. Vary, *Heavy Quarkonium in a Holographic Basis*, *Phys. Lett. B* **758** (2016) 118 [[1509.07212](#)].
- [79] Y. Li, P. Maris and J.P. Vary, *Quarkonium as a relativistic bound state on the light front*, *Phys. Rev.* **D96** (2017) 016022 [[1704.06968](#)].
- [80] S. Tang, Y. Li, P. Maris and J.P. Vary, *B_c mesons and their properties on the light front*, *Phys. Rev. D* **98** (2018) 114038 [[1810.05971](#)].
- [81] M. Li, Y. Li, G. Chen, T. Lappi and J.P. Vary, *Light-front wavefunctions of mesons by design*, [2111.07087](#).
- [82] S. Tang, Y. Li, P. Maris and J.P. Vary, *Heavy-light mesons on the light front*, *Eur. Phys. J. C* **80** (2020) 522 [[1912.02088](#)].
- [83] W. Qian, S. Jia, Y. Li and J.P. Vary, *Light mesons within the basis light-front quantization framework*, *Phys. Rev. C* **102** (2020) 055207 [[2005.13806](#)].
- [84] S. Jia and J.P. Vary, *Basis light front quantization for the charged light mesons with color singlet Nambu–Jona-Lasinio interactions*, *Phys. Rev. C* **99** (2019) 035206 [[1811.08512](#)].
- [85] BLFQ collaboration, *Transverse structure of the pion beyond leading twist with basis light-front quantization*, *Phys. Lett. B* **839** (2023) 137808 [[2301.12994](#)].

- [86] Y. Li and J.P. Vary, *Longitudinal dynamics for mesons on the light cone*, *Phys. Rev. D* **105** (2022) 114006 [[2202.05581](#)].
- [87] BLFQ collaboration, *Light mesons with one dynamical gluon within basis light-front quantization*, in *19th International Conference on Hadron Spectroscopy and Structure*, 1, 2022 [[2201.05987](#)].
- [88] BLFQ collaboration, *Angular momentum and generalized parton distributions for the proton with basis light-front quantization*, *Phys. Rev. D* **105** (2022) 094018 [[2202.00985](#)].
- [89] BLFQ collaboration, *Transverse momentum structure of proton within the basis light-front quantization framework*, *Phys. Lett. B* **833** (2022) 137360 [[2205.04714](#)].
- [90] BLFQ collaboration, *Nucleon structure from a light-front hamiltonian*, *Rev. Mex. Fis. Suppl.* **3** (2022) 0308111.
- [91] S. Xu, C. Mondal, X. Zhao, Y. Li and J.P. Vary, *Nucleon spin decomposition with one dynamical gluon*, [2209.08584](#).
- [92] B. Wu, *Factorization and transverse phase-space parton distributions*, *JHEP* **07** (2021) 002 [[2102.12916](#)].
- [93] Y.V. Kovchegov and E. Levin, *Quantum chromodynamics at high energy*, vol. 33, Cambridge University Press (8, 2012), [10.1017/CBO9781139022187](#).
- [94] A.H. Mueller, *Soft gluons in the infinite momentum wave function and the BFKL pomeron*, *Nucl. Phys. B* **415** (1994) 373.
- [95] A.H. Mueller and B. Patel, *Single and double BFKL pomeron exchange and a dipole picture of high-energy hard processes*, *Nucl. Phys. B* **425** (1994) 471 [[hep-ph/9403256](#)].
- [96] A.H. Mueller, *Unitarity and the BFKL pomeron*, *Nucl. Phys. B* **437** (1995) 107 [[hep-ph/9408245](#)].
- [97] Y.V. Kovchegov, *Inclusive gluon production in high energy onium-onium scattering*, *Phys. Rev. D* **72** (2005) 094009 [[hep-ph/0508276](#)].
- [98] M. Habich, G.A. Miller, P. Romatschke and W. Xiang, *Testing hydrodynamic descriptions of $p+p$ collisions at $\sqrt{s} = 7$ TeV*, *Eur. Phys. J. C* **76** (2016) 408 [[1512.05354](#)].
- [99] R.D. Weller and P. Romatschke, *One fluid to rule them all: viscous hydrodynamic description of event-by-event central $p+p$, $p+Pb$ and $Pb+Pb$ collisions at $\sqrt{s} = 5.02$ TeV*, *Phys. Lett. B* **774** (2017) 351 [[1701.07145](#)].

- [100] W. Zhao, Y. Zhou, K. Murase and H. Song, *Searching for small droplets of hydrodynamic fluid in proton–proton collisions at the LHC*, *Eur. Phys. J. C* **80** (2020) 846 [[2001.06742](#)].
- [101] M.L. Miller, K. Reygers, S.J. Sanders and P. Steinberg, *Glauber modeling in high energy nuclear collisions*, *Ann. Rev. Nucl. Part. Sci.* **57** (2007) 205 [[nucl-ex/0701025](#)].
- [102] B. Wu and Y.V. Kovchegov, *Time-dependent observables in heavy ion collisions. Part I. Setting up the formalism*, *JHEP* **03** (2018) 158 [[1709.02866](#)].
- [103] PARTICLE DATA GROUP collaboration, *Review of Particle Physics*, *PTEP* **2022** (2022) [083C01](#).
- [104] T. Hahn, *CUBA: A Library for multidimensional numerical integration*, *Comput. Phys. Commun.* **168** (2005) 78 [[hep-ph/0404043](#)].
- [105] T. Hahn, *Concurrent Cuba*, *J. Phys. Conf. Ser.* **608** (2015) 012066 [[1408.6373](#)].
- [106] J.-Y. Ollitrault, *Anisotropy as a signature of transverse collective flow*, *Phys. Rev. D* **46** (1992) 229.
- [107] Y.I. Azimov, Y.L. Dokshitzer, V.A. Khoze and S.I. Troyan, *Similarity of Parton and Hadron Spectra in QCD Jets*, *Z. Phys. C* **27** (1985) 65.